The Cala Viola-Torre del Porticciolo coastal area: a key tectono-stratigraphic site to unravel the polyphase tectonics in NW Sardinia

Niccolò Menegoni[1], Angelo Cipriani[2], Rudy Scarani[3], Lorenzo Stori[4], Paolo Citton[5], Marco Romano[6], Umberto Nicosia[6] & Ausonio Ronchi[3]

[1] Ali I. Al-Naimi Petroleum Engineering Research Center (ANPERC), King Abdullah University of Science and Technology (KAUST), Thuwal, Saudi Arabia.
[2] Dipartimento per il Servizio Geologico d'Italia - ISPRA, Roma.
[3] Dipartimento di Scienze della Terra e dell'Ambiente, Università di Pavia, Pavia, Italy.
[4] Dipartimento di Scienze della Terra, dell'Ambiente e della Vita, Università di Genova, Genova, Italia.
[5] IIPG, Instituto de Investigación en Paleobiología y Geología (CONICET - UNRN), General Roca, Río Negro, Argentina.
[6] Dipartimento di Scienze della Terra, Sapienza Università di Roma, Roma, Italy.

NM, 0000-0003-2857-4930; AC, 0000-0002-3971-3177; PC, 0000-0002-6503-5541; MR, 0000-0001-7629-3872; UN, 0000-0001-6429-1685; AR, 0000-0002-7158-3990.

Ital. J. Geosci., Vol. 143, No. 1 (2024), pp. 75-104, 16 figs., https://doi.org/10.3301/IJG.2024.05.

Research article

Corresponding author e-mail: rudy.scarani.geo@gmail.com

Citation: Menegoni N., Cipriani A., Scarani R., Stori L., Citton P., Romano M., Nicosia U. & Ronchi A. (2024) - The Cala Viola-Torre del Porticciolo coastal area: a key tectono-stratigraphic site to unravel the polyphase tectonics in NW Sardinia. Ital. J. Geosci., 143(1), 75-104, https://doi.org/10.3301/IJG.2024.05.

Associate Editor: Giulio Viola
Guest Editor: Simone Fabbi

Submitted: 16 May 2023
Accepted: 4 November 2023
Published online: 06 December 2023

SUPPLEMENTARY MATERIAL is available at: https://doi.org/10.3301/IJG.2024.05

ABSTRACT

Along the coast between Cala Viola and Cala del Turco in NW Sardinia, an upper Palaeozoic to lower Mesozoic continental sedimentary succession is wonderfully exposed. For the first time, detailed geological mapping, coupled with facies analysis and meso-structural studies, was carried out, allowing to better define the Permian-Triassic stratigraphy and structural setting of this sector of Nurra region. Field work was coupled with drone-based aerial photogrammetry, which led to the production of Digital Outcrop Models (DOMs). A lithofacies subdivision of the stratigraphic units is proposed with the aim of making a formalisation of the Triassic Porticciolo conglomerate and Cala Viola sandstones units possible. The combination of "classical" and "digital" field methodologies led to the mapping of 462 faults, the recognition and characterisation of six main fault sets, and differently oriented folds. The analysis of topology and cross cutting relationship of fault networks has allowed us to identify at least eight deformation phases, possibly spanning from Permian to Pleistocene-Holocene. These new data allow us to reconstruct the complex tectonic history affecting NW Sardinia since the deposition of the middle Permian deposits to the Holocene, with the Permian and Triassic deposits recording the whole deformation phases affecting them since the latest Palaeozoic.

KEY-WORDS: geological mapping, structural geology, stratigraphy, Permian, Triassic, Sardinia.

INTRODUCTION

Since the end of the 19th century, the continental succession of Nurra has been a subject of significant interest for numerous researchers. The area has drawn attention due to its remarkable geological exposures (e.g., Lovisato, 1884; Oosterbaan, 1936; Pecorini, 1962; Vardabasso, 1966; Gasperi & Gelmini, 1980; Fontana et al., 1982) and its subsurface deposits (Pomesano Cherchi, 1968; Pittau Demelia & Flaviani, 1982; Pittau & Del Rio, 2002). Over the past three decades, the long-known "*Permotriassic*" continental and volcanic deposits, cropping out along the NW Sardinia coast to the north of Alghero, have regained attention due to new stratigraphic petrographic and palaeontological studies (Cassinis et al., 1996; Cortesogno et al., 1998; Fontana et al., 2001; Sciunnach, 2001; Cassinis & Ronchi, 2002; Cassinis et al., 2002, 2003; Costamagna, 2012; Gaggero et al., 2017). Furthermore, other studies have delved into the content of Aluminium Phosphate Sulfate (APS) minerals in the upper portion of the section (Borruel-Abadia et al., 2019) and explored the palaeomagnetism of the Permian and Triassic red beds (Bachtadse et al., 2018) to gain deeper insights into the geological history of the Nurra region and its interregional correlation (e.g., Bourquin et al., 2011; Gretter et al., 2015; Schneider et al., 2020). Despite the significant knowledge acquired in recent years, the stratigraphic framework of the Nurra region still needs major deepening and knowledge. Moreover, unlike E and SW Sardinia, which have been extensively studied in a geodynamic and tectonic context, the Nurra region has received relatively little attention in this

regard (e.g., Oggiano et al., 2015; Casini et al., 2020). The exposure of the upper Palaeozoic-lower Mesozoic sedimentary cover overlying the Variscan crystalline basement provides a valuable opportunity to identify and reconstruct the tectonic-stratigraphic history of this part of Sardinia, with deposits recording the entire sequence of deformation phases since the latest Palaeozoic. For this reason, we undertook a comprehensive tectonostratigraphic investigation of the Permian and Triassic succession exposed along the Torre del Porticciolo coastal area. Our study integrates palaeontological, stratigraphic and structural analyses to achieve a deeper geological understanding of the Nurra region. We combined traditional and innovative techniques, including detailed field mapping at the 1:5,000 scale, acquiring mesoscale structural data and observations, constructing and analysing 3D models using the drone-based aerial photogrammetric survey.

We propose a redefinition of the stratigraphic framework in the study area, partly already achieved through the lithostratigraphic correlation with SE France (Toulon-Cuers Basin, Provence), with new lithofacies subdivisions. This redefinition is further supported by new palaeontological findings, and radiochronometric and palaeomagnetic studies. By improving the knowledge of the stratigraphic succession and its approximative age, we obtain crucial insights into the complex temporal and spatial sequence of tectonic phases that affected the region from the Permian to the late Caenozoic times. This integrated approach allows us to interpret and untangle the local geological history more accurately, while providing important clues for the reconstruction of the tectonic history of the Sardinian-Corso block.

The study area (Figs. 1, 2) is located in the Nurra region of NW Sardinia, along the north coast of the Capo Caccia promontory. Along this coastal section, from Punta del Gallo to the south up to the relief of Punta Lu Caparoni to the north, the most complete lower Permian to Middle Triassic succession of the island is wonderfully exposed.

GEOLOGICAL SETTING

Sardinia exhibits a geological setting characterised by Variscan crystalline rocks (both metamorphic and intrusive) overlain by upper Palaeozoic-Caenozoic siliciclastic, calcareous and volcaniclastic deposits. The NW sector of Sardinia (i.e., the Nurra region) records a complex tectono-stratigraphic history, reflecting the evolution of this (palaeo-)sector of the European continent since the Palaeozoic.

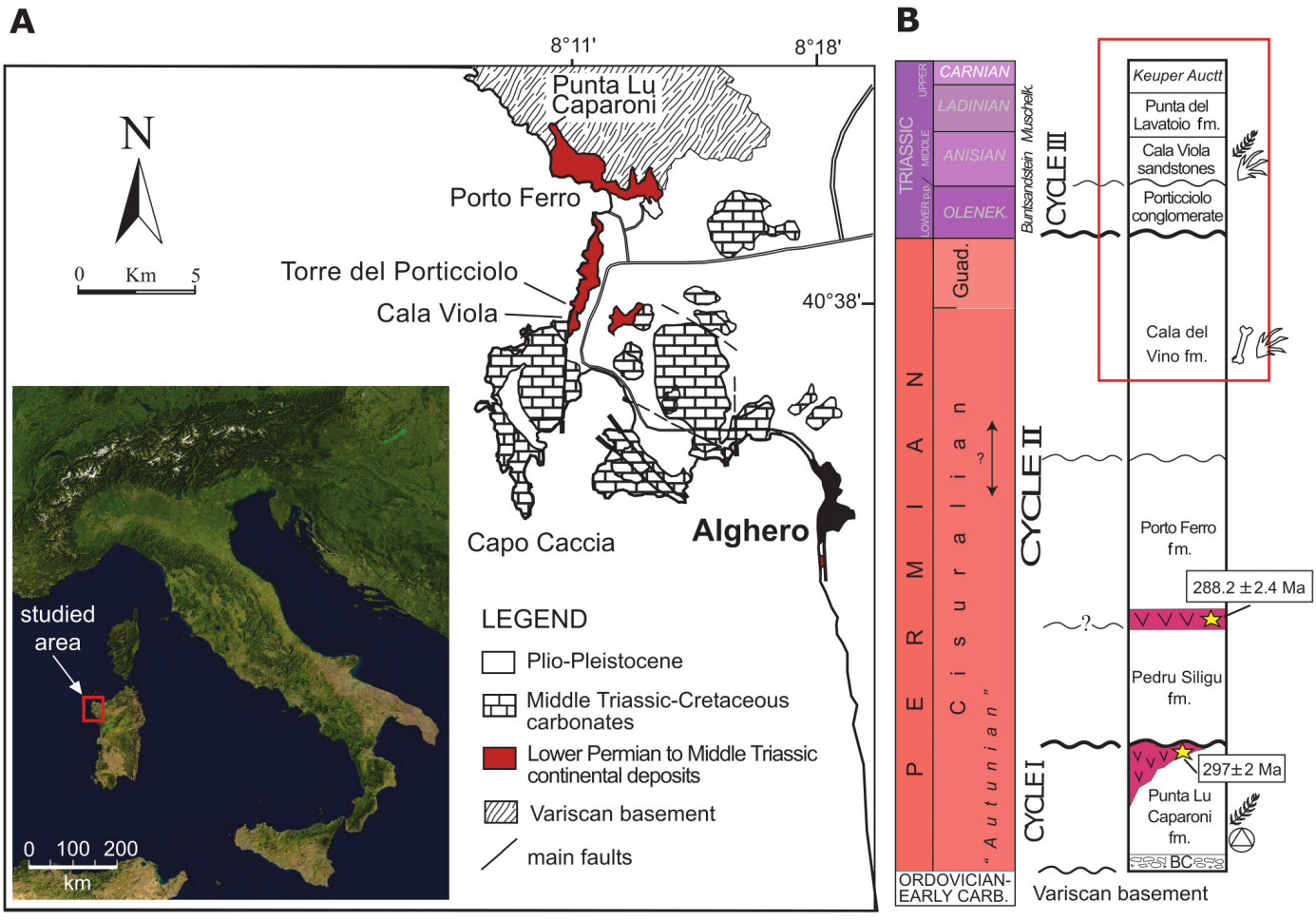

Fig. 1- Geographic and geological setting of the study area. (a) Location sketch map of the main geologic units north of Alghero and up to Argentiera Massif (Nurra). (b) Simplified stratigraphic section of the Permian and Triassic continental and Middle-Upper Triassic marine to transitional deposits in the type area.

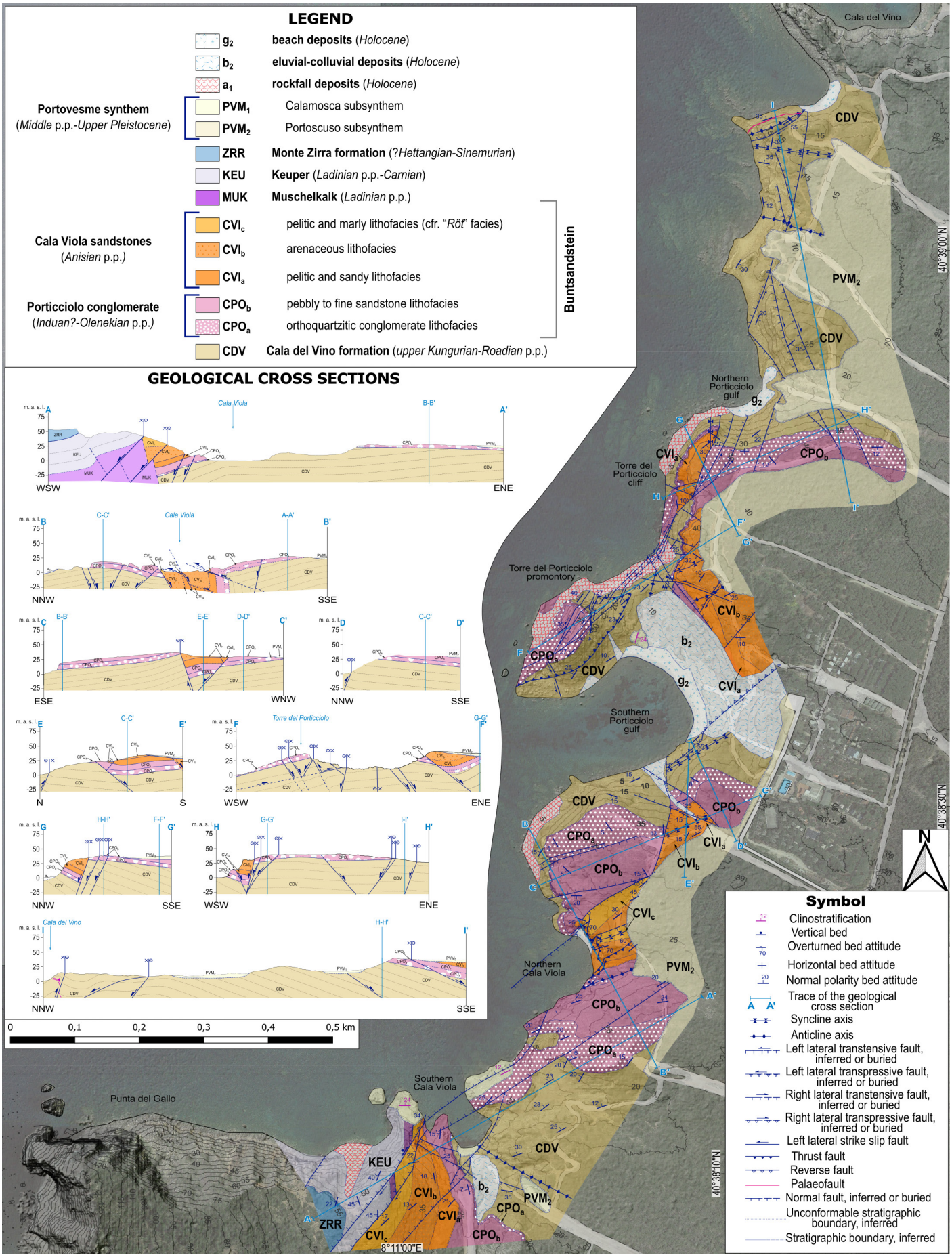

Fig. 2 - Geological map of the Cala Viola-Cala del Vino area simplified from the main map in S1.

The crystalline basement is part of the South-European Variscan orogen and experienced intrusions of huge masses of igneous rocks during the late Variscan phase, triggered by the gravitational collapse of the accretionary wedge (for a comprehensive review, see Carmignani et al., 2001). Subsequent post-orogenic extensional tectonics dismembered the orogenic belt, leading to the formation of narrow, fault-bounded fluvial-lacustrine basins that evolved into more extensive alluvial environments, alongside the emplacement of effusive volcanic rocks. Evidence of this is observed in the lower Permian-Middle Triassic siliciclastic deposits unconformably overlaying the Variscan substrate and intercalated with volcaniclastic deposits (Gaggero et al., 2017).

The Tethyan rifting also influenced this part of the southern European margin, as evidenced by the deposition of evaporitic and thick shallow-water platform carbonates during the Mesozoic and the lower part of the Caenozoic. Subsequently, the Eocene to Holocene sedimentary record is represented by continental, marine and volcanic deposits.

The entire post-Variscan sedimentary cover exhibits evidence of both compressive and transcurrent deformations, related to the Alpine/Apennine orogenic phases, as well as extensional deformations associated to the opening of the Balearic and Tyrrhenian basins (e.g., Carmignani et al., 1994, 2001; Funedda et al., 2000; Oggiano et al., 2018).

Permian and Triassic stratigraphy of the Nurra

In the last thirty years, renewed studies on the area allowed to subdivide the early Permian to Middle Triassic evolution of the Nurra continental succession into at least three major sequences or tectono-stratigraphic units (TSUs), separated by marked unconformities (Cassinis & Ronchi, 2002; Cassinis et al., 2002, 2003).

The first sequence (TSU1) lies non-conformably over the Variscan crystalline basement and formed essentially during the earliest Permian. It is represented by the thin (up to 15 m) Punta Lu Caparoni formation (Gasperi & Gelmini, 1980), composed of fine-grained black lacustrine deposits with conglomeratic and sandy fluvial intercalations locally overlain by quartz-rich ignimbrites (V_1; 297±1.8 Ma; Gaggero et al., 2017). Rich earliest Permian palaeofloras ("Autunian" *auctt.*) were reported by various authors (Pecorini, 1962; Gasperi & Gelmini, 1980; Ronchi et al., 1998).

The second sequence (TSU2) has an estimated thickness of ca. 600 m, probably extending from part of early Permian (Sakmarian?) up to late Kungurian-Roadian? times (Ronchi et al., 2011). Deposits characterising this sequence consist of three stacked continental, unconformity-bounded, formations (hereafter referred to as Pedro Siligu, Porto Ferro and Cala del Vino fms.), clustered in an informal group-rank lithostratigraphic unit ("Nurra Group" by Ronchi et al., 2011). From the base to the top these are:

- the Pedru Siligu fm. (Cassinis et al., 2002, 2003; cfr. "unit 1" by Gasperi & Gelmini, 1980), at the base of TSU2 and made of ~50 m of channelised conglomerate and sparse sandstone typical for braided alluvial environments. This unit covers with a slight angular unconformity the Punta Lu Caparoni fm. and is followed locally by ignimbrite deposits (V_2; 288±2.4 Ma; Gaggero et al., 2017);
- the Porto Ferro fm. (Cassinis et al., 2002, 2003; cfr. "unit 2" by Gasperi & Gelmini, 1980), consisting of fluvial grey-reddish coarse sandstone and polygenic conglomerate with clasts deriving from both the preceding volcanic episode and the metamorphic substrate. The total estimated thickness of the unit is about 150-200 m. The Porto Ferro fm. is barren of fossils but, based on its stratigraphic position, has been generally assigned to the late Cisuralian-early Guadalupian time interval. This age is also supported by an interregional correlation with the Les Salettes Fm. of southern Provence (Toulon-Cuers Basin), in which a latest lower Permian-?middle Permian macro- and microfloral association occurs (Bau Rouge Member; Durand, 2006, 2008);
- the Cala del Vino fm. (Cassinis et al., 2002, 2003; cfr. "unit 3" by Gasperi & Gelmini, 1980), up to more than 300 m in thickness, characterised by an alternation of grey-brown, medium- to coarse-grained sandstone and violet-red siltstone-claystone, with an upward coarsening trend to pebbly sandstone and polygenic conglomerate.

The third sequence (TSU3) begins with typical continental to transitional Buntsandstein deposits (Lower-Middle Triassic), starting with a thin quartz conglomerate ("*Conglomerato del Porticciolo*", hereafter Porticciolo conglomerate - Cassinis et al., 2002, 2003; Costamagna, 2012; cfr. the Provencal *Poudingue de Port-Issol* by Glinzboeckel & Durand, 1984; Durand et al., 1989; Durand, 2006, 2008) that overlies the Cala del Vino fm. through a regional low-angle angular unconformity. This erosional surface coincides with a significant gap encompassing *pro parte* the Guadalupian up to the late Early Triassic. The Porticciolo conglomerate is followed by fluvial, fine-to-coarse grained, reddish sandstone ("*Arenarie di Cala Viola*", *sensu* Pittau Demelia & Flaviani, 1982; Cassinis et al., 2002, 2003; hereafter Cala Viola sandstones). The upper part of this unit is characterised by yellowish sandstone and grey-green marly pelite bearing halite pseudomorphs ("*Röt* facies" *Auctt.*). Detrital modes of the single units of the Permian and Triassic succession can be found in Cassinis et al. (1996) and Sciunnach (2001).

Middle Triassic carbonate deposits are referred to the Muschelkalk (Pittau Demelia & Flaviani, 1982; Cherchi & Schroeder, 1985; Pittau & Del Rio, 2002) and reach up to a maximum of 180 m in thickness (Cugiareddu well - Pomesano Cherchi, 1968), and are in turn overlain by the evaporitic deposits of Keuper (Bornemann, 1881; Lovisato, 1884).

Tectonics

Sardinia experienced a complex tectonic history (Carmignani et al., 2001; Zattin et al., 2008), spanning from the Ordovician (Cocco et al., 2018) to the Pleistocene-Holocene (Casini et al., 2020). Following the Variscan orogeny (Carmignani et al., 1994), transtensional-extensional tectonics, associated with late Palaeozoic-Mesozoic rifting, resulted in the collapse of the Sardinia segment of the Variscan chain (Ziegler & Stampfli, 2001). The Permian-Triassic syn-rift continental succession documents an early stage of intracontinental rifting (Cassinis et al., 1980).

Subsequently, during the Jurassic (Bajocian?–Bathonian), extensional tectonics mainly affected eastern Sardinia (Zattin et al., 2008). In the Aptian-Albian time interval, the northwestern part of Sardinia experienced extensional tectonics, leading to the reactivation of inherited ENE-WSW late Variscan structures (in present day coordinates) as normal faults (Oggiano et al., 2018). During the Late Cretaceous, compressive-transpressive tectonics generated NNE-SSW trending sinistral strike-slip faults (in present day coordinates), associated with gentle folds and minor normal faults (Oggiano et al., 2018).

Since the Palaeogene to the Middle Miocene, a series of different tectonic events, commonly referred to as the Pyrenaic phase (Cherchi & Trémolières, 1984; Barca & Costamagna, 1997), occurred (Carmignani et al., 1992, 2001, 2004; Oggiano et al., 2018). Oggiano et al. (2018) demonstrated that, unlike in SW-Sardinia, the majority of folds of NW-Sardinia trend NE-SW accommodating NW-SE shortening. Due to the absence of clear stratigraphic markers, these deformation phases may be attributed not only to the Pyrenaic phase, but also to an Oligocene-earliest Miocene (i.e., Aquitanian) phase. The latter, possibly ascribable to the Apennines orogeny (Carmignani et al., 1994; Oggiano et al., 2009), is manifested by sinistral transcurrent faults with ENE-WSW trends that generate a series of transtensive basins and minor transpressive structures (Oggiano et al., 2018).

Subsequently, a new extensional event occurred in the Burdigalian, generating NNW-SSE striking normal faults, which may have led to the deepening of the Porto Torres basin towards the E (Funedda et al., 2000; Oggiano et al., 2018). In addition, this regime activated conjugate E-W and WNW-ESE trending and N-dipping normal faults, such as the San Martino fault (Oggiano et al., 2018). Consequently, the Sardinian-Corsican Block was affected by a drifting phase toward SE, contributing to the opening of the Balearic Basin. Afterwards the opening of the oceanic floor changed the drift direction of the Sardinian-Corsican Block from SE to E, maximising its counterclockwise rotation and the general tilting of Nurra to NE (Fanucci et al., 2001; Oggiano et al., 2018).

According to Oggiano et al. (2018), two additional extensional tectonic phases occurred during the Neogene: a Serravalian event generating high-angle normal faults with E-W strikes, and a Pliocene extensional phase, which produced and reactivated near-vertical normal faults with N-S and NE-SW orientations.

Furthermore, the recent luminescence analysis conducted by Casini et al. (2020) revealed an extensional event of Late Pleistocene-Holocene age that reactivated the pre-existing faults with strikes ranging from NW-SE and NNE-SSW. Specifically, in the Cala Viola area reactivation of the Le Bombarde and Porto Ferro faults, during MIS7 and MIS5, respectively, has been inferred. Despite that, no evidence of tectonic activity in historical times (the last 1000 years) is documented by the Catalogue of Italian Earthquakes (Postpischl, 1985) and the Parametric Catalogue of Italian Earthquakes (CPTI - Rovida et al., 2022), as well as no seismogenic sources are reported in the Database of Individual Seismogenic Sources (DISS, 2021) and ITaly HAzard from CApable faults (ITHACA, 2019).

MATERIAL AND METHODS

To reconstruct the tectonics and stratigraphy of the study area we employed a combination of classical field and digital methodologies.

High-resolution geological mapping, using a lithostratigraphic approach, was performed to re-evaluate and define the stratigraphic and structural features of the Cala Viola-Cala del Vino area. We enlarged the *Carta Tecnica Regionale* (CTR) of Sardinia region, originally at the 1:10,000 scale (available online), to the 1:5,000 scale, which served as base map for the geological mapping.

To acquire mesostructural data on folds and faults, we collected "punctual" field measurements at specific structural stations. These measurements allowed us to perform a kinematic analysis and (palaeo-)tectonic reconstruction of the area. The software FaultKin v. 8.1.2 (Allmendiger et al., 2012; https://www.rickallmendinger.net/faultkin) was used to process the collected field data.

To digitalise the main geological map (see Supplementary Material I - S1) and generate graphical representation, we used the open-source software QGIS v. 3.20.3 Odense (https://qgis.org/en/site/) and InkScape v. 1.1 (https://inkscape.org/), respectively.

We performed a photogrammetric survey using two Unmanned Aerial Vehicles (UAVs): DJI Phantom 4 RTK (P4RTK) and DJI Mavic Air 2 (MA2) quadcopters. Using the software Agisoft Metashape v. 1.6 (Agisoft LCC, available at https://www.agisoft.com/) and following the methodology described by Menegoni et al. (2022a), we generated Digital Outcrop Models (DOMs). The DOMs were, then, analysed following Menegoni et al. (2022b) and Panara et al. (2022), employing the open-source software CloudCompare (retrievable at http://www.cloudcompare.org/), as well as Pluraview 28 UHD stereoscopic device. For further details on the UAV survey and DOMs, please refer to Supplementary Material II (S2).

FIELD DATA

Stratigraphy

In this section the main stratigraphic and sedimentological features of the mapped units are described, mainly based on previous works (Fontana et al., 2001; Cassinis et al., 2002, 2003; Ghinassi et al., 2009; Ronchi et al., 2011; Costamagna, 2012). In the light of a future stratigraphic formalisation (in progress) of the two Triassic continental units (i.e., Porticciolo conglomerate and Cala Viola sandstones), we propose here a novel subdivision into different mappable lithofacies, describing their main features (see Fig. 3). The need of such a new subdivision is explained hereafter in sub-chapter 6.1. The mapped lithostratigraphic, informal (i.e., lithofacies) and unconformity-bounded units are:

- **Cala del Vino formation (CDV):** this formation is represented by grey-green to light brown channelised sandstone bodies decreasing upwards in thickness and lateral continuity, interbedded with greyish and dark-red finer material (Fig. 4a).

The large, laterally persistent, sheet sand bodies can be related to meander-belt deposits laid down by medium-scale

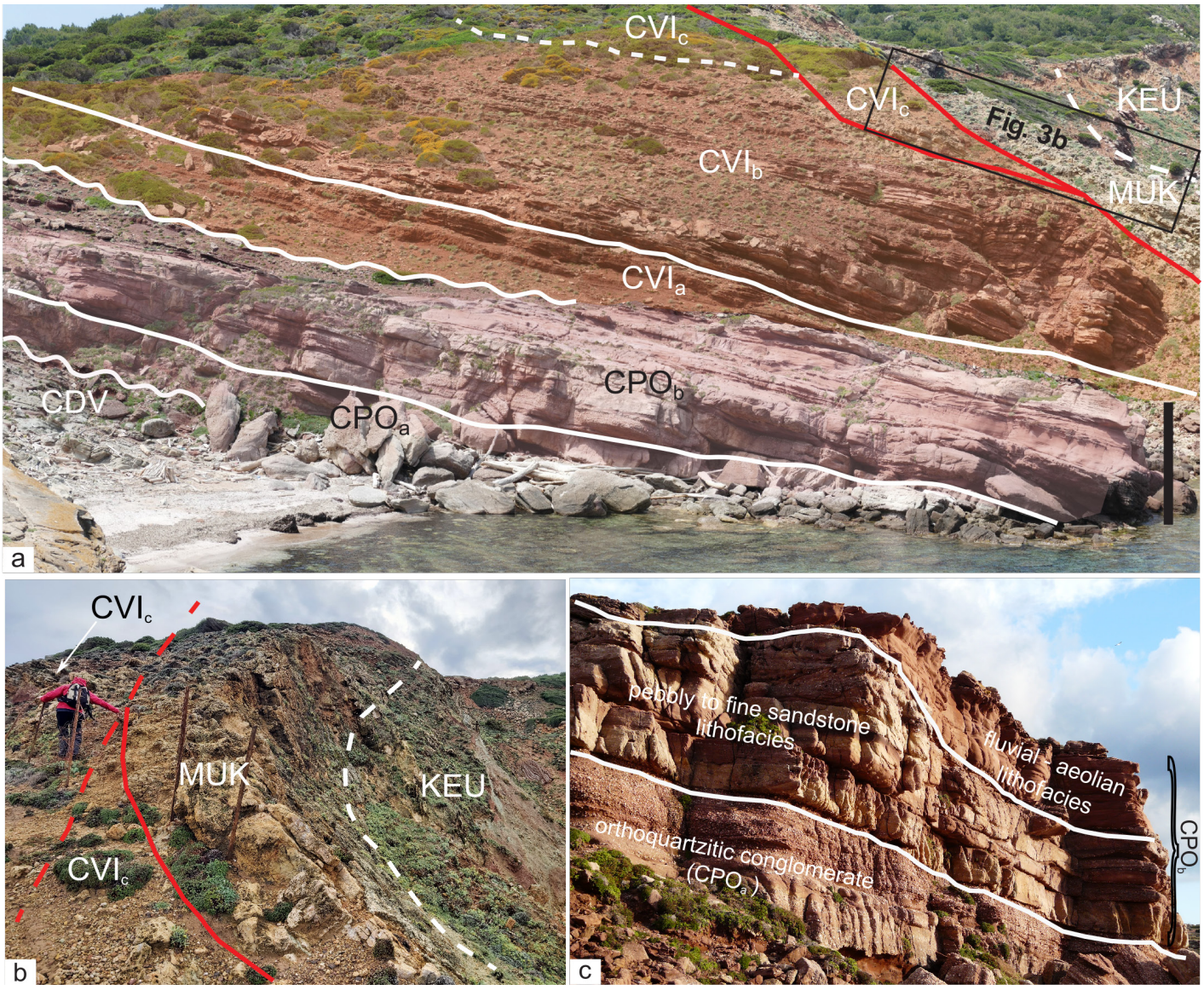

Fig. 3 - Main lithofacies subdivision of Porticciolo conglomerate and Cala Viola sandstones. (a) Cala Viola south section. Scale bar to the right is 5 metres. (b) Stratigraphic and tectonic contacts of Muschelkalk dolomicrites (MUK) with Keuper (KEU) evaporitic facies and with the Röt-like "marly and pelitic lithofacies" of Cala Viola sandstones (CVI$_c$), respectively (Cala Viola south section). (c) Porticciolo conglomerate with its 2 lithofacies subdivision in the southern Porticciolo gulf: CPO$_a$ gravel braided orthoquarzitic conglomerates; CPO$_b$: pebbly to fine sandstones. This last lithofacies comprises two different portions: mostly pebble sandstones with fine sandstones intercalations (below) and fine to coarse sandstones with fluvial-aeolian facies (above).

streams. They are composed of medium- to coarse-grained sandstone and show frequent trough- and planar-cross bedding, parallel lamination with ripple cross-lamination and lenticular channel fills with a marked erosional base over the overbank facies (Fig. 4a, b). Sheet-like sandstone with planar cross-bedding and parallel laminations, characterised by poor lateral continuity, is also intercalated with the channel-fill bodies and can be interpreted as crevasse-splay deposits of various size and scale. The overbank floodplain facies, dark red to purple in colour, are represented by levee sandstone and siltstone up to claystone (Fig. 4a, b). They appear as pervasively burrowed (see Baucon et al., 2014) and are commonly structureless, except for pedogenic features, like colour mottling and carbonate concretions. Sandstone bodies can reach up to 2 metres in thickness, whereas the red fine-grained deposits range from a few cm up to 4-5 metres.

CDV is the oldest mapped unit and its base is not exposed, whereas the mapped thickness of the formation was evaluated to be at least 200 metres. The unit passes upward to the Porticciolo conglomerate through a paraconformity or a low-angle angular unconformity (Fig. 4a), representing a major break (*sensu* Miall, 2016) encompassing the Guadalupian *p.p.* to Early Triassic *p.p.* time span. Pre-Triassic tectonics (see below) deformed the CDV deposits, locally causing their tilting and uplift. The subsequent Triassic peneplanation phase led to the exhumation of older CDV facies in uplifted sectors. As a result, the deposits underlying the unconformity between CDV and the younger Porticciolo conglomerate show different ages moving laterally. In the study sector of the coast, a stratigraphically lower part (i.e., uplifted) of CDV is covered by the Triassic Porticciolo conglomerate. To the NNE of the northern Porticciolo gulf up to Porto Ferro, the coastal area offers a long section through the CDV with good exposure,

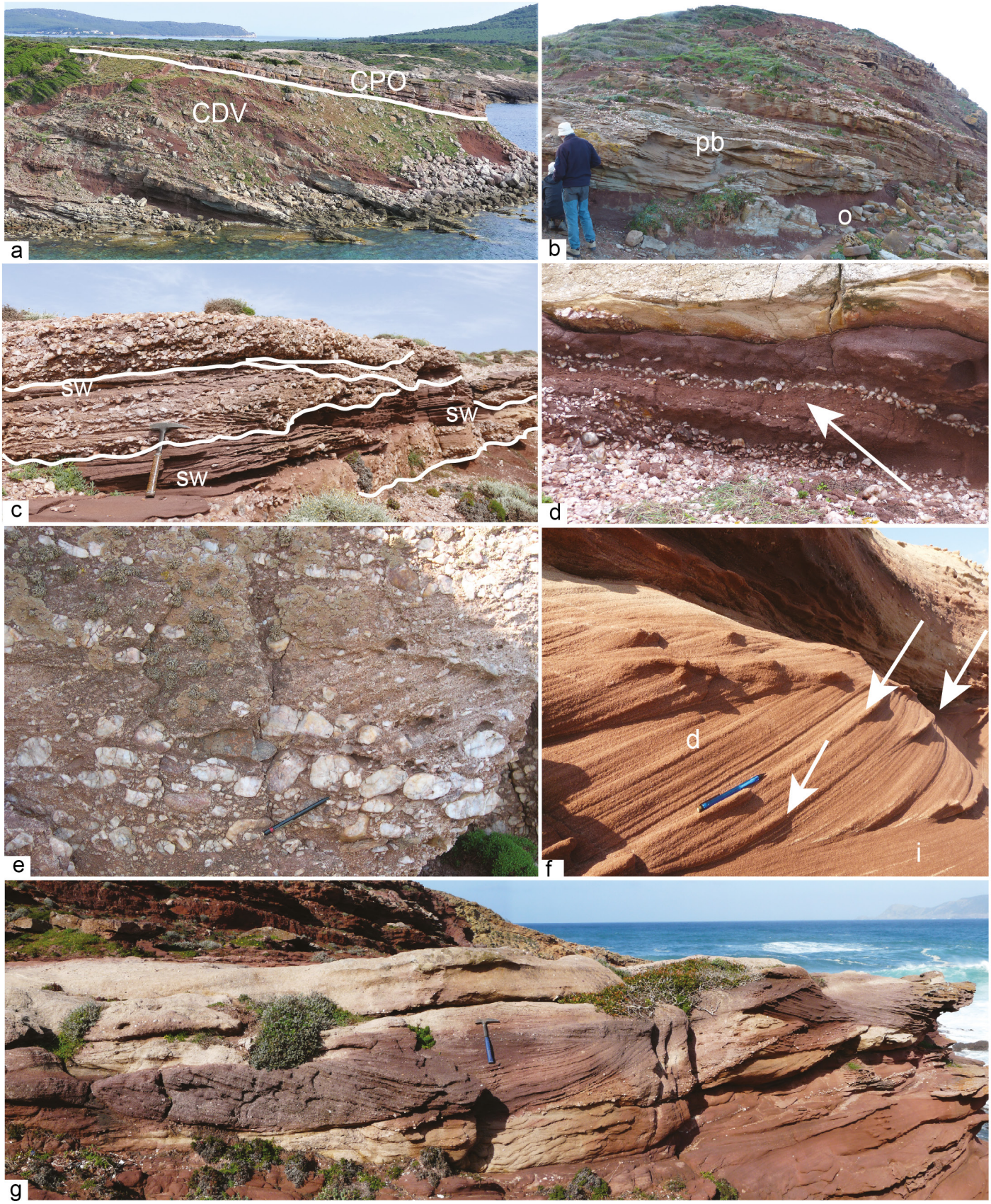

Fig. 4 - Field view of the Cala del Vino fm. and Porticciolo conglomerate, and relative lithofacies. (a) Panoramic view of southern Porticciolo gulf showing the unconformable contact between the Permian Cala del Vino (CDV) and the Triassic Porticciolo conglomerate (CPO) formations. Note the alternation of sandy fluvial bars and pelitic overbank facies in CDV deposits. (b) A fluvial point bar in the CDV (pb) overlying overbank reddish pelites (o). (c) Tightly-packed breccia/conglomerate beds with an erosive base intercalated to sand wedges (sw) in the CPO_a lithofacies. (d) Palaeo-reg with in-situ strings of ventifacts (arrow), inside medium size reddish sandstones in lithofacies CPO_b. (e) Clast-supported pebbly conglomerates (inclined pen for scale, showing imbrication) in CPO_a lithofacies. (f) Aeolian dunes in CPO_b lithofacies with dune-interdune laminations (arrows show grain flow episodes). (g) Large scale fluvial trough-cross stratification in upper part of lithofacies CPO_b.

practically continuous for more than 300 m; its monoclinal structure (dipping to the north) allows to show a marked coarsening–upward trend, which is the same progradational trend shown by the corresponding Saint-Mandrier fm. in the Toulon area (Durand, 1993, 2006, 2008). No age indications are to-date provided by this last unit, whereas the CDV is assigned to latest Cisuralian – early Guadalupian on the basis of its palaeontological record.

- Porticciolo conglomerate (CPO): this formation consists of 8-12 m-thick well sorted milky quartz-conglomerate, vertically evolving to cross-bedded coarse- to very coarse whitish, red and purple sandstone (Cassinis et al., 2002, 2003). Costamagna (2012) firstly proposed a detailed sedimentologic description and a facies subdivision of this unit. In our view, the sedimentary products of this formation can be clearly subdivided in two characteristic lithofacies in the field (Fig. 3c), mainly reflecting changes in depositional mechanisms, namely an **orthoquartzitic conglomerate lithofacies (CPO_a)** and a **pebbly to fine sandstone lithofacies (CPO_b).** The latter shows a lower and an upper portion (Fig. 4c-e):

- **orthoquartzitic conglomerate (CPO_a)**: a mostly chaotic, quartz conglomerate displaying a crudely plane-parallel stratification and a moderate to well-developed coarsening upward trend (Fig. 4c, e), mainly referable to a wadi braided system. Pebbles, in some cases imbricated (Fig. 4c), are mostly sub-rounded and are normally pluricentimetric, reaching diameters >10 cm. The conglomerate is usually massive and clast-supported, but matrix-supported facies do also occur and the vein-quartz elements are dispersed in a reddish sandy or silty matrix (Fig. 4c). They are related to longitudinal bars, which generated coarsening upward units as result of downcurrent migration of the coarse bar head on the finer bar tail (Ghinassi et al., 2009). Cross-stratified clast-supported pebbly to cobbly conglomerate, possibly related to the development of transverse to diagonal bars or to the infill of erosive scours, is present, though rare (Ghinassi et al., 2009). Several channel-like bodies can be observed, most of which are filled with cross-stratified sandy-conglomerate, or locally with sandstone and mudstone lenses or wedges. A massive, locally mottled, muddy interval bearing strings of *in situ* ventifacts (palaeo-regs; Fig. 4d) and poorly developed palaeosol is located at the top of the informal unit and separates the CPO_a from CPO_b in the southern Porticciolo cliffs (Fig. 4a). The pebbles show a typical fabric resulting from fluvial transport over a long distance, interrupted by long periods of aeolian wear (i.e., ventifacts, see Bourquin et al., 2007; Durand & Bourquin, 2013). They testify to a clearly arid or hyper-arid climate, which was brought to the fore at many other places in Europe and probably started around the latest Early Triassic (Smithian-Spathian: Durand, 1988; Durand et al., 1989; Bourquin et al., 2007). This conglomeratic lithofacies abruptly overlies the CDV siltstones and claystones and can be followed from the southern cliffs of Cala del Vino to Cala Viola, *via* its type locality (i.e., Porticciolo area). The unconformity between CDV and CPO_a coincides with a disconformity or low-angle angular unconformity marking a significant stratigraphic gap of about 15 Myr. The thickness of this lithofacies ranges from a few decimetres in the southern Cala Viola sector to 3 metres.
- **pebbly to fine sandstone lithofacies (CPO_b)**: the lower part of this unit is characterised by pebbly to fine sandstone. These gravelly sandstone fluvial braided, mostly tabular deposits overlie the previous massive conglomeratic lithofacies. Geometries of the channels are not visible but, nonetheless, well developed cross-stratifications, locally indicating a transport oblique to the main dip of beds, could suggest the establishment of relatively sinuous channels. Locally, a decimetric interval of dark red siltstone-claystone separates this quartz-cemented coarse-grained sandstone and pebbly to conglomeratic sandstone from the underlying orthoconglomeratic lithofacies. The pebbly to fine sandstone is well-stratified, cross-bedded to plane-bedded, and small laminated aeolian dunes are intercalated. This facies association is about 6 metres thick. The upper part of the facies is characterised by purple fine very well-sorted quartz-sandstone related to small aeolian dunes/interdunes, showing a clear distinction between grain flow and grain fall laminae (Fig. 4f), and, at the top, pebbly to coarse sandy deposits reworked in fluvial or wadi settings (Fig. 4g). This facies association is markedly sandy and contains very well-preserved sedimentary structures (e.g., tabular cross and trough cross-stratification in the finer, aeolian facies and trough-cross stratification in the coarser, fluvial facies). Unfortunately, the limited exposure prevents from defining channel geometries and bar dynamics. The thickness of this upper part of CPO_b is about 4 metres.

The Porticciolo conglomerate is considered Olenekian *p.p.* in age (e.g., Durand et al., 2006, 2008; Borruel-Abadia et al., 2019) and passes to the overlying Cala Viola sandstones through a paraconformity. The boundary is also marked by an abrupt lithological change, coincident with a variation in the fluvial sedimentation style very likely related to a change in climatic conditions.

- Cala Viola sandstones (CVI): consists of medium-to-fine reddish sandstone, siltstone and mudstone deposited in terminal fans setting by relatively sinuous channels, developed under semi-arid conditions (Cassinis et al., 2003; Durand, 2006, 2008). Due to its lithological features, well exposed in the type locality of Cala Viola and along the cliff north of Torre del Porticciolo, this formation has been subdivided in three mappable lithofacies:

- **pelitic and sandy lithofacies (CVI_a)**, consisting of dark orange-red siltstone and sandstone packages, up to 1 metre thick, separated by 0.3-1 metre thick discontinuous muddy intervals containing abundant, both *in situ* or reworked pedogenic concretions (Fontana et al., 2001; Cassinis et al., 2002; Ghinassi et al., 2009). The geometry of sandstone bodies is not clearly visible at the outcrop scale, but they show an erosive base, commonly floored by pluricentimetric thick intraformational fine breccias made up of reworked pedogenic materials (e.g., carbonate concretions) and mud clasts. These coarse-grained layers are in turn capped by a

fining-upward succession grading from coarse sandstone to sandy mudstone. The complete intervals can be interpreted as inundate sequences (Fig. 5e; Durand, 2008). This facies is typical of floodplain-to-playa deposits. Each depositional unit, less than 1 metre thick, is sheet-like in the lower part and tends to take a biconvex lens shape in the upper part. The rest of the section is rich in red-coloured floodplain-to-playa deposits characterised mainly by kappa cross-stratification in fine to very fine sandstone (Fig. 5b; Durand, 2008); there, sandstone bodies become plano-convex and can be interpreted as terminal-fan lobes deposited by ephemeral streams (Durand, 2008). This lithofacies overlies with sharp facies change the CPO_b. The contact between the two formations is represented by a 2-3rd order unconformity (likely the Hardegsen unconformity; Bourquin et al., 2007). This lithofacies is up to 5 metres thick.

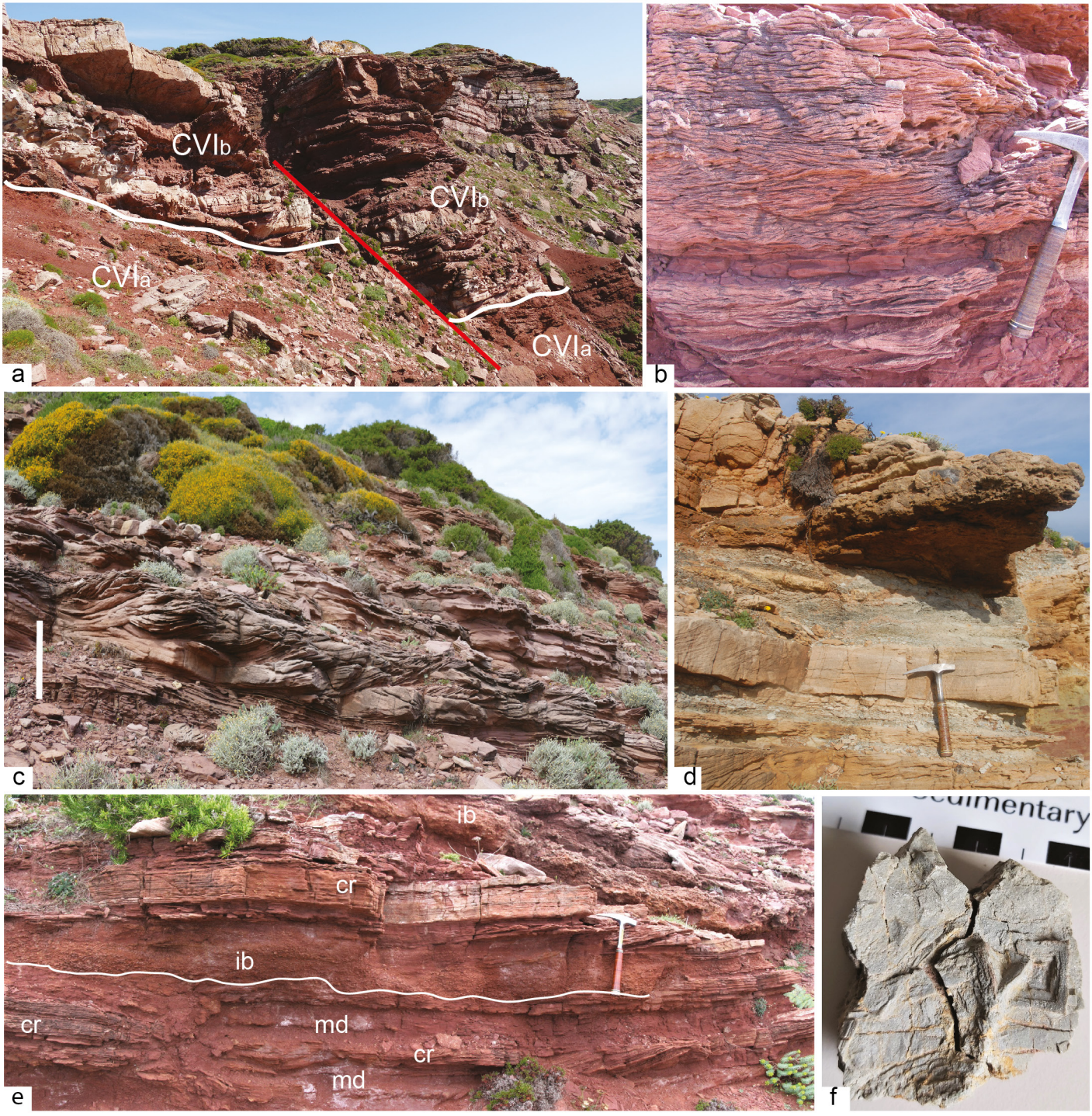

Fig. 5 - Field view of the Cala Viola sandstones lithofacies. (a) Panoramic view of the Torre del Porticciolo cliff where the stratigraphic passage between CVI_a and CVI_b is spectacularly exposed. (b) Climbing ripples in CVI_a (kappa-cross of Allen, 1963). (c) Cross-stratified medium sandstones in the upper part of CVI_b. (d) Alternation of yellow-brownish cross-stratified sandstone bars and grey-greenish mudstones (CVI_c). Scale bar: approx. 1 metre. (e) Repeated flood sequences in CVI_a (md: mud drapes; ib: intraformational breccias; cr: climbing ripples). (f) Grey-greenish platy mudstones with cubic halite cast in CVI_c.

- **arenaceous lithofacies (CVI_b)**, represented by tabular beds with good lateral continuity and morphological relief of medium to coarse-grained reddish sandstone (Fig. 5a), characterised by well-developed ripple cross-laminations, clay chips and subordinate plane parallel and trough cross-stratifications. The uppermost part of this lithofacies is characterised by red, orange and purple, cm- to dm-thick, fine to medium sandstone and siltstone, interspaced with mudstone. Cross bedded sets of this lithofacies (Fig. 5c) were also interpreted by Costamagna (2012) as sequences of tidal rhythmites cut by migrating sand bars and tidal channels of various sizes showing lateral accretion. Thick planar lamination in coarse sandstones also occurs. The main dip of beds (~NW) is almost transverse to the main palaeotransport direction (~SW in present day coordinates), as highlighted by the trough cross-stratification in the lower part of the channel. In this case, the occurrence of laterally accreting bars (point bar?) could be proposed (Ghinassi et al., 2009). This lithofacies is about 14 metres thick.
- **pelitic and marly lithofacies** (cfr. "*Röt*" facies) **(CVI_c)**, characterised by *Röt*-like yellow-greenish sandstone (bearing halite-crystal casts; Fig. 5f), marl and polychrome claystone occurring at the top of the unit. Distinctive is the progressive change in colour from green to yellowish in the upper part of the facies where large scale planar cross stratification alternates with grey-greenish finely laminated mudstones (Fig. 5d). This unit crops out only at the top of southern Cala Viola and in the very deformed zone of northern Cala Viola (see Fig. 2 and the Main Map in S1). Estimated thickness is >10 metres.

The thickness of the Cala Viola sandstones has been estimated in geological cross sections of more than 30-40 metres; this conservative value is related to the lack of exposure of the upper stratigraphic boundary in the study area (mainly due to tectonics). The age of the unit is Anisian *p.p.*

- Muschelkalk (MUK): in the Cala Viola section, few metres of yellowish dolomicrite and dolomitic limestone with carniolar porosity probably due to dissolution of evaporites, are ascribed to the uppermost part of the Muschelkalk, which passes gradually to the Keuper facies. The Muschelkalk carbonates, which mark the Middle Triassic marine ingression, crop out for about some tens of metres in the classic Monte Santa Giusta or Punta del Lavatoio sections (Alghero). In the Cala Viola section, almost all the Muschelkalk, as well as most of the *Röt*-like facies on top of Cala Viola sandstones (CVI_c) were tectonically displaced and are thus missing. The age of the unit is Ladinian *p.p.*, as constrained by its high palaeontological content (ammonoids, conodonts, palynomorphs, bivalves and algae), whereas the passage to the overlying unit is transitional and marked by the occurrence and increase of supratidal marine and muddy sabkhas deposits.

- Keuper (KEU): this formation is characterised by red, green and yellowish marl and claystone bearing gypsum intercalations. These plastic, evaporitic and dolomitic deposits are tectonically disturbed and crop out in the southernmost sector of the Cala Viola coast (Ghiscera Mala locality). The fossiliferous content of the Keuper is very poor except for microfloristic associations ascribed to the late Ladinian-Carnian (Pittau Demelia & Del Rio, 1980), and it is difficult to provide a detailed description of the whole stratigraphic unit. In its lower part, it is possible to observe strongly folded gypsiferous shales with euhedral quartz and carniolar dolomite. In its upper part, grey and brecciated dolostone with thin intercalations of reddish to greenish claystone and thinly bedded dolomitic layers showing microbialitic laminations, occur.

The age is Ladinian *p.p.*-Carnian by literature and the stratigraphic passage to the overlying Mt. Zirra fm. is abrupt and marked by the occurrence of light-coloured, massive limestone.

- Mt. Zirra formation (ZRR): this formation represents the youngest mapped Mesozoic unit in the area. It is characterised by yellowish to whitish ooidal, peloidal and oncoidal limestone bearing quartz and arenaceous lithic clasts, alternated with yellow dolostone, marl and sandstone (Fig. 6a-b). The main textures are grainstones and packstones, bearing bioclasts (bivalves, gastropods, corals, benthic foraminifers, echinoids, green algae). Beds range from decimetric to metric in thickness and are tabular to lensoidal in geometry (Fig. 6b). Sedimentary structures like tractive plane-parallel and through-cross laminations locally occur. The mapped thickness of the unit is about 30 metres, but the whole thickness is more than 150 metres by literature. In the absence of a detailed biostratigraphic study for this unit (out of the scope of this work), the age of the deposits is assigned to the Early Jurassic (?Hettangian-Sinemurian) by the literature (Oggiano et al., 2018).

The development of a shallow water carbonate platform environment in the Early Jurassic persisted at least up to the Late Cretaceous, as marked by peritidal conditions of carbonates characterising the Capo Caccia promontory (e.g., Oggiano et al., 2018).

- Portovesme synthem (PVM): this unit is represented by the Middle-Upper Pleistocene deposits covering unconformably the Palaeozoic-Mesozoic *p.p.* bedrock. According to Oggiano et al. (2018) and to the sheet 459 "Sassari'' of the Geological Map of Italy at 1:50,000 scale (CARG Project – Servizio Geologico d'Italia, 2018), contiguous to the study area, this synthem was subdivided in two subsynthems based on the genesis of the involved deposits. The Authors relate to the MIS6 glacial phase the unconformity bounding in the lower part of this UBSU, whereas the upper unconformity coincides with the actual topographic surface. By contrast, Andreucci et al. (2006, 2010) and Casini et al. (2020) refer *pro parte* the deposits of the Portovesme synthem to the Middle Pleistocene (MIS7). Consequently, the erosive phase that produced the basal unconformity bounding this synthem should be older than MIS6.

- **Calamosca subsynthem (PVM_1):** to this unit are assigned several shallow-marine lithofacies (calcarenitic, calciruditic and bioclastic deposits), accumulated in shoreface and beachface settings of small pocket beaches (Andreucci et al., 2006, 2010; Casini et al., 2020). Centimetric and decimetric, subrounded to subangular, clasts of the local Palaeozoic-Mesozoic bedrock are associated with bioclasts (mainly gastropods, bivalves and red

Fig. 6 - (a) Panoramic view of the southern part of the study area, facing the Capo Caccia promontory. Here, the stratigraphic boundary between KEU and ZRR is exposed. (b) Detail of Fig. 6a, where the coarse-grained carbonates of ZRR overly sandy-silty deposits of KEU. Hammer as a scale. (c) Field view of the unconformity between the Pleistocene mixed carbonate-siliciclastic sandy deposits of PVM_1 and faulted sandstones and siltstones of CDV at northern Porticciolo gulf. Hammer as a scale. (d) Metric blocks accumulated as rockfall deposits at the toe of the Torre del Porticciolo cliff.

algae) and are cemented by carbonate cement, forming polygenic and heterometric conglomerates and breccias. Associated are also calcarenite-calcirudite formed by terrigenous coarse-grained sand (Fig. 6c), locally by pockets of pebbles, coupled with fragments and whole shells of bivalves and gastropods. The deposits are well-cemented and are clinobedded towards the sea. These Quaternary deposits coincide with the historical "*panchina Tirreniana" Auct.* and have been found from the actual beach shore to the topographic height of 15 m and are up to 10 metres thick.

- **Portoscuso subsynthem (PVM_2)**: this UBSU encompasses from a few decimetres up to a few metres of well-sorted sand and sandstone, yellowish in colour, resting unconformably on the Permian-Triassic bedrock and, locally, on the Pleistocene PVM_1. These continental deposits display through-cross bedding and are referable to large-scale aeolian dunes.

- Rockfall deposits (a_1): monogenic and polygenic diamicton related to the gravitational collapse and backstepping of the steep cliffs characterising the study area (Fig. 6d). These Holocene deposits can reach thicknesses of a few metres and mainly occur at the toes of the cliffs that are eroded by the wave action and/or by violent sea storms.

- Eluvial-colluvial deposits (b_2): represented by sandy and silty sediments related to the *in situ* alteration of the Holocene soil, bearing coarser clasts sourced from the exposed bedrock. In the study sector, eluvial-colluvial deposits are mainly related to the alteration of the Permian and Triassic siltstones and claystones, and of the Pleistocene aeolian deposits of PVM_2. These reddish deposits, up to a couple of metres in thickness, are ubiquitous.

- **Beach deposits (g_2)**: sandy to pebbly sediments bearing bioclasts (fragments or whole specimens of molluscs and echinoids).

Palaeontology

Vertebrate palaeontology

A renewed interest in the palaeontological content of the Permian and Triassic deposits appeared starting in 2008, when a student of the University of Pavia discovered eight vertebrae of a large tetrapod still in articulation and partially embedded in the red Permian sediments cropping out in the Torre del Porticciolo promontory (CDV). The finding immediately proved to be of great importance, especially considering the total absence at the time of osteological remains from the Nurra sedimentary succession.

In fact, fossil remains from the area appear to be historically rare, despite intensive studies in the last decades, and were represented only by micro and macro-floral fossils found in the basal portion of the Punta Lu Caparoni Fm. (see Pecorini, 1962; Gasperi & Gelmini, 1980; Ronchi et al., 1998) indicating a middle "Autunian" age, and in the upper portion of CVI, suggesting an Early Triassic age (Pecorini, 1962).

Since 2008, a team of the Department of Earth Sciences of Sapienza, University of Rome, in collaboration with the University of Pavia, has conducted over 16 field campaigns in the area, leading to the discovery, *in situ* taphonomic study, collection and preparation of over eighty osteological elements (both whole and fragmentary), referable to a significant new member of the Family Caseidae. After an initial report (Ronchi et al., 2008), a detailed description of the geology of the area and of the taphonomy of the fossil site at Torre del Porticciolo Promontory (TdP1) was presented by Ronchi et al. (2011). That paper also provides a first brief description and representation of some recovered osteological elements, mostly ribs, vertebrae and some autopodial elements. The latter, especially the phalangeal elements, indicate a great affinity of the specimen with the huge North American caseids, leading to a first dubious attribution of the new specimen as ?*Cotylorhynchus* sp. Stovall, 1937 and suggesting a late Kungurian–Roadian age for the upper part of the CDV (Ronchi et al., 2011).

All material collected until 2014 was analysed in detail for the first time by Romano & Nicosia (2014) who, based on the autapomorphic characters recognised with respect to large North American caseids, formalised the new taxon of the Family Caseidae *Alierasaurus ronchii* (Romano & Nicosia, 2014). *A. ronchi* is characterised by vertebrae and ribs totally consistent to those of the large North American caseids, whereas the more autapomorphic elements are represented by the pedal phalanxes (Romano & Nicosia, 2014). The new caseid was characterised by a very wide 'barrel-shaped' rib cage, which is typical of high-fibres herbivorous diet, hosting long intestinal tracts for celluloses and hemicelluloses digestion (Hotton et al., 1997; Sues & Reisz, 1998; Reisz & Sues, 2000; Lombardo, 2008; Romano & Nicosia, 2014, 2015; Romano, 2017a). The total length of the body reconstructed by Romano & Nicosia (2014) must have exceeded six metres, a value comparable if not greater than the giant North American caseid *Cotylorhynchus hancocki*.

Further postcranial material of *A. ronchi* collected after 2014 from the TdP1 site has been figured and described in detail by Romano et al. (2017). The authors also explored for the first time the phylogenetic position of the new taxon within Caseidae, using as a basis a recently published cladistic analysis of the Family (Romano & Nicosia, 2015; Brocklehurst et al., 2016). The achievement of enormous body size in *Alierasaurus* was probably made possible by the presence, already in the less derived and smaller taxa, of "overbuilt" long bones (*sensu* Romano, 2017b; Romano & Rubidge, 2019), linked to the digging behaviour of these Permian herbivores (Romano, 2017b).

A second fossiliferous site (Torre del Porticciolo 2, TdP2) was found during fieldwork in 2015 about one hundred metres away from the original caseid productive site and can be essentially referred to the same stratigraphic level (Romano et al., 2019). During several post 2016 campaigns, several hundreds of both complete and fragmentary bones have been recovered, found still embedded in the red sediments of the Cala del Vino formation and in the debris formed by the recent erosion of the productive deposits. Romano et al. (2019) conducted a detailed taphonomic analysis showing that all the osteological elements can be likely referred to a single individual and proposed a complex and multiphasic taphonomic history for the remains (at least four main phases from the death of the individual to its present finding).

Based on the peculiar structure of the left maxilla, Romano et al. (2019) proposed a possible preliminary attribution to the carnivorous group of Sphenacodontidae. A detailed study of the new specimen could provide important information, considering that sphenacodontids are essentially known from the Permian beds of the south-western United States, and the new specimen from Italy could shed crucial light on the dispersal and occurrence of the predaceous Permian Family in the European continent.

Vertebrate ichnology

Permian tetrapod tracks from CDV were recovered from a stratigraphic horizon very close to TdP1 and TdP2 (Citton et al., 2019). Footprints, ranging in total length from 4 cm to 10 cm, were assigned to *Merifontichnus* isp., strongly resembling tracks named *Merifontichnus thalerius* by Gand et al. (2000) from the upper Guadalupian La Lieude Formation (see Michel et al., 2015 for temporal constraints). These footprints most likely anticipate the occurrence of *Merifontichnus* to the Roadian, after rejection of previous reports from different ages (Citton et al., 2019), and suggest producers of up to one metre in total body length as member of the terrestrial palaeofauna, to be added to the giant *Alierasaurus ronchii* Romano & Nicosia, 2014 and the indeterminate sphenacodontid from TdP1 and TdP2.

Tetrapod footprints of Triassic age were also recovered from the middle-upper portion of CVI. All the footprints are minute, being less than 3 centimetres in total length, and show two distinct morphologies that supported assignment to the ichnogenera *Rhynchosauroides* Maidwell, 1911 and *Rotodactylus* Peabody, 1948, most likely produced by prolacertiforms and dinosauromorph, respectively (Citton et al., 2020).

Invertebrate ichnology

The Permian and Triassic continental succession of Nurra sheds light on decapod crustaceans, because it preserves the oldest (Roadian) fluvial *Ophiomorpha*? and *Camborygma*, ascribed to ghost shrimps (Decapoda: Axiidea, Gebiidea) and crayfishes (Decapoda: Astacidea, Parastacidea), respectively (Baucon et al., 2014). These crustacean trace fossils are part of a well-preserved ichnofauna including *Arenicolites*, *Diplocraterion*, *Helminthoidichnites*, *Palaeophycus*, *Planolites*, rhizoliths, *Skolithos*, *Spongeliomorpha*, *Taenidium*, *Treptichnus*, alongside an undetermined tetrapod footprint, helical burrows and *Sinusichnus*-like traces (Baucon et al., 2014). Most of these invertebrate trace fossils are found in the Permian CDV with a dramatic reduction in the Triassic Porticciolo conglomerate and a renewed occurrence in the CVI (Baucon et al., 2014).

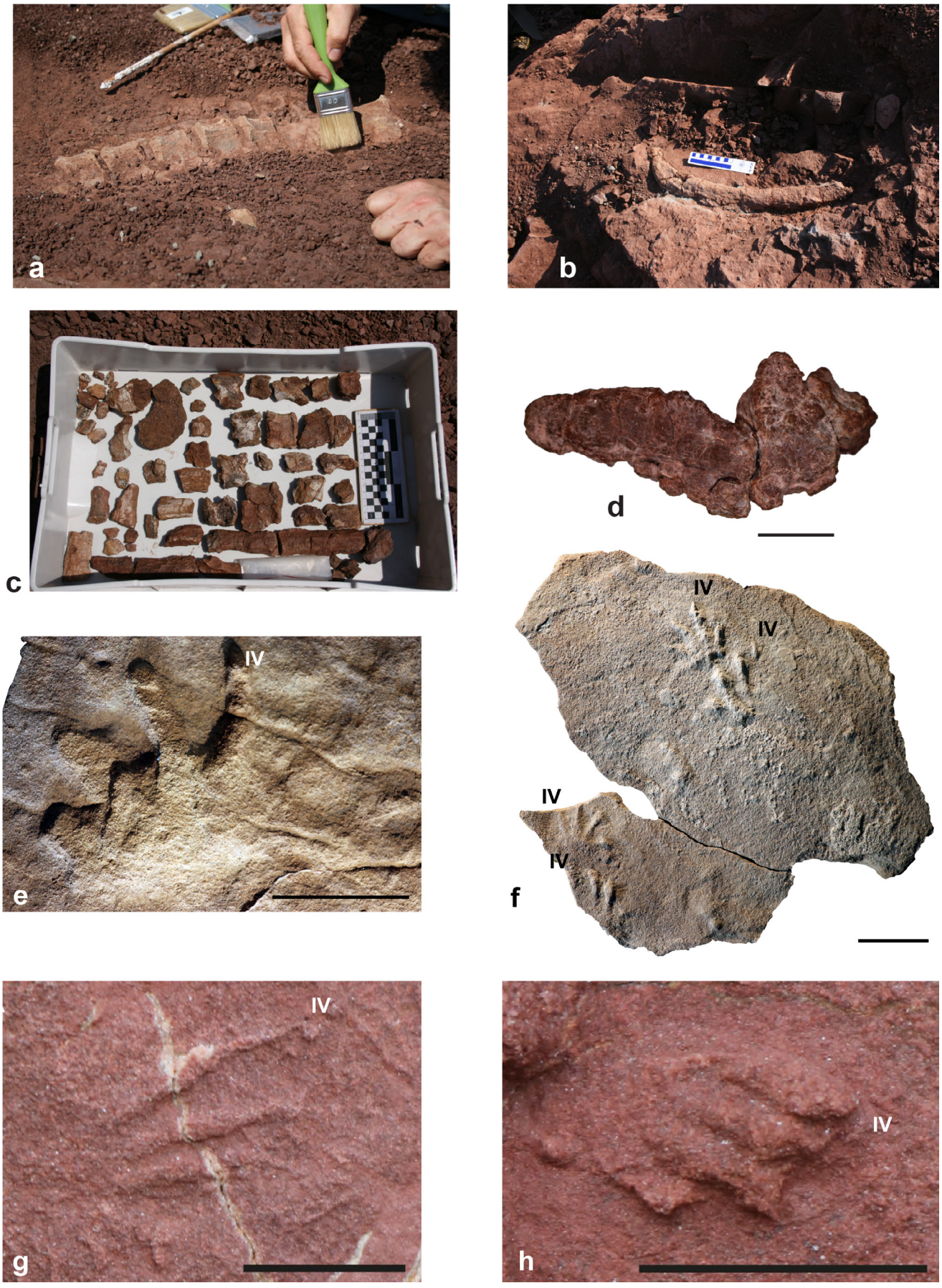

Fig. 7 - Tetrapod body- and ichnofossil record from NW Sardinia. a) Articulated caudal vertebrae in right lateral view of *Alierasaurus ronchii*; b); c); d) NS 166/8. Right maxilla in lateral view from TdP2 site; e, f) Footprints referred to *Merifontichnus* isp. from Cala del Vino fm. (TdP3 site). g, h) Footprint referred to *Rhynchosauroides* isp. (g) and *Rotodactylus* isp. (h) from Cala Viola sandstones. Roman numerals identify digit IV impression. Scale bars 5 cm (e, f) and 1 cm (g, h).

Macro-microfloras

In the CDV rhizoliths and stems of trunks occurred in the sandstone bars, but no macro-or microflora remains were found to-date. Up to now the only macrofloristic data recorded on the upper part of the Permian and Triassic siliciclastic sequence of Nurra (now related to the CVI) are those found by Pecorini (1962), who reported the presence, in arenaceous-clayey layers at Cala Viola, of equisetales referable to *Equisetum mougeotii* Brongt. and as well as some estherias. Thus, this author refers the uppermost deposits of the "Permotriassic" sequence to an Early Triassic age. Vegetation induced sedimentary structures (centroclinal cross-strata and creeping-stem moulds from Equisetites) are the expression of discontinuous plant cover. In the gypsiferous shales of KEU at Ghiscera Mala (south of Cala Viola) an upper Ladinian-Carnian palynological association was reported by Pittau Demelia & Del Rio (1980).

Structural geology

Outcrop description

Below, we present a description of the most distinctive outcrops, proceeding from the northern to the southern region (Fig. 8, see also Fig. 2 for the reported localities).

- Cala del Vino-northern Porticciolo gulf area

The northern sector of the mapped area exhibits extensive exposures of CDV and the unconformity with the overlying Porticciolo conglomerate. The CDV sandstone and siltstone is displaced by mesoscopic faults displaying dip-slip normal displacement. These structures have an approximate E-W strike and dip towards N and S at angles between 8-25° (Fig. 9a-b).

Such faults are involved in the hanging wall anticline of a high-angle, right-lateral transpressive fault striking ENE-WSW and dipping towards NNE. These normal faults are exposed in the northern limb (backlimb) of the fold, which dips towards NNW at approximately 35°. Assuming that the bedding attitude of the deposits involved by the normal faulting had been horizontal and, in turn, deformed by the compressive deformation, the restoration of the original attitudes reveals the previous southward dip of these normal faults. This fault is not only folded but also cut by the younger transpressive deformation structures (Fig. 9a; see also geological cross section I-I' in Fig. 2 and S1). Associated to this right-lateral compressive lineament is a set of synforms and antiforms in the footwall block, striking approximately ESE-WNW (Fig. 2). A main NNE-striking and WNW-dipping left-lateral transtensional fault, associated with antithetic, right-lateral NNW-trending R' Riedel structures, displaces the folds affecting the Permian rocks.

In the northern Porticciolo gulf, the SSE-dipping siltstone and sandstone of CDV (dip angle ~ 20°) is overlain by the sub-horizontal Triassic conglomerate of CPO_a (Fig. 9c). The Permian beds are truncated by an erosional surface at the base of CPO_a and display toplap terminations of 20°; the angular unconformity appears to be exposed with an apparent dipping in this locality. This stratigraphic relationship provides information about the occurrence of a deformation phase between the deposition of CDV and CPO_a, resulting in the tilting of Permian beds with respect to the Triassic ones.

The entire area is affected by several sinistral transtensional faults, which can be grouped into two different sets: the first one with an orientation of 293N/75°, the second one with an orientation of 255N/62°. The main fault displaces the succession by about 25 metres (vertical stratigraphic displacement), juxtaposing the CVI facies directly on CDV; associated with these faults are also oblique-slip duplexes, one of which is exposed along the northern termination of the Torre del Porticciolo cliff and preserves a block of Triassic conglomerates (CPO_a) interposed between CDV and CVI (at the footwall and the hanging wall, respectively – enlargement in Fig. 9c).

The faults appear to be sealed by the Pleistocene marine and continental deposits of the Portovesme synthem.

- Torre del Porticciolo cliff

The approximately 200 metre long cliff north of the Torre del Porticciolo promontory provides a spectacular exposure of the local uppermost part of CDV, the unconformity with the Porticciolo conglomerate, and most of the CVI (Fig. 10), along with several tectonic features. The sedimentary succession generally dips towards SE at about 10-15°, but the dip angle increases to 30° in the hanging wall of the most prominent structure in this area. Here, a high-angle left-lateral transtensional fault, trending NNE-SSW and dipping towards WNW at 55°, represents the southern extension of the sinistral fault detected in the northern Porticciolo gulf (Fig. 10a; refer to geological cross sections G-G' and H-H' in Fig. 2 and S1). The slip surface is exposed on the crest of the cliff in the form of a fault scarp, primarily resulting from the rheological contrast between the rocks in the hanging wall (CVI) and those in the footwall (CPO_a), but no clear slickensides were identified. The

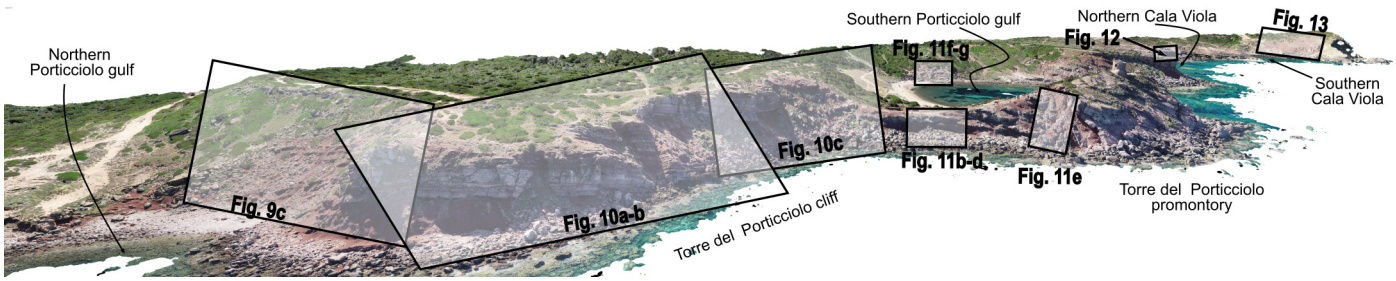

Fig. 8 - DOM of the study area from the north in which the selected outcrops are highlighted.

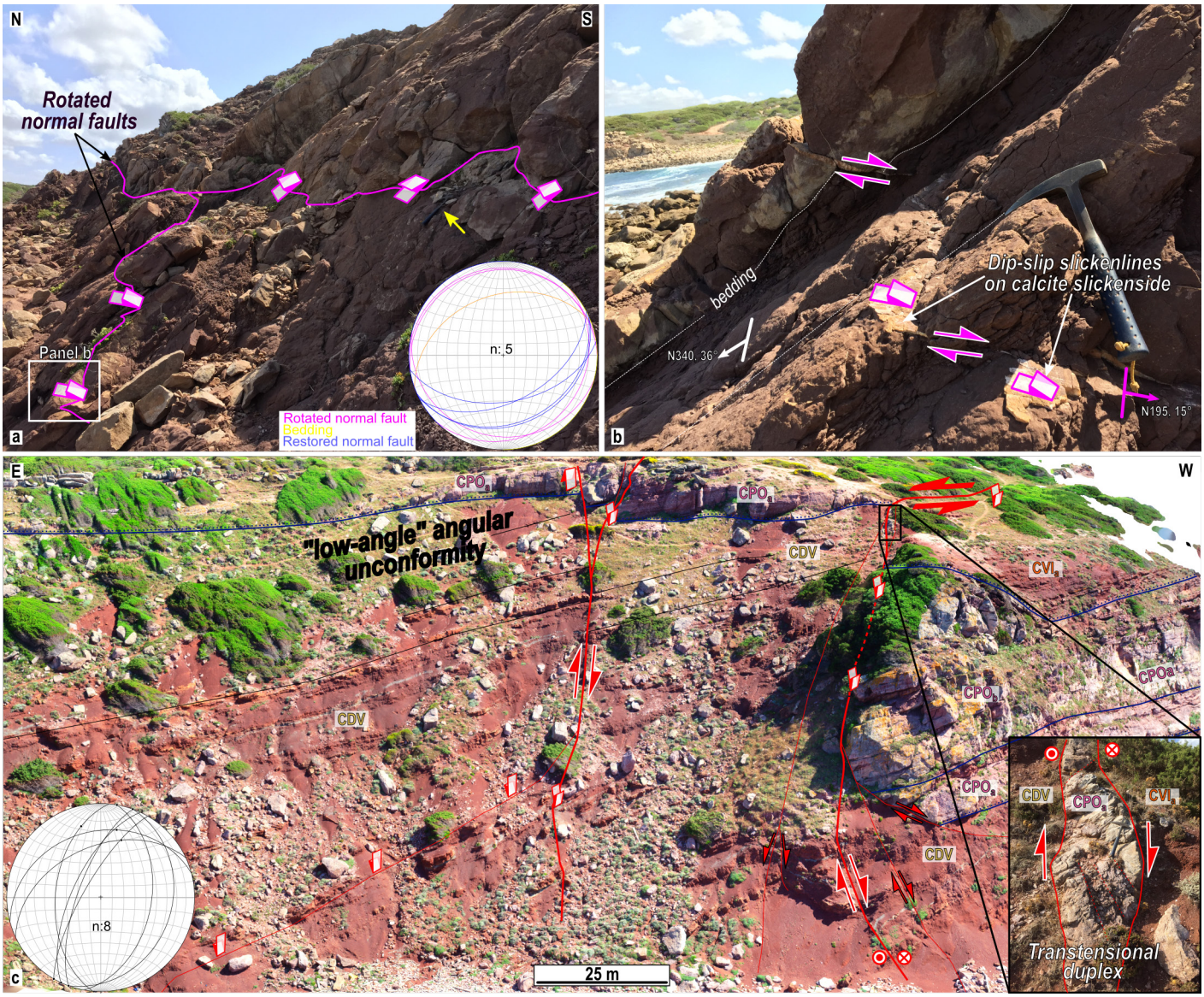

Fig. 9 - (a)(b) Photographs details of the mesoscopic faults displaying dip-slip kinematics and normal displacement visible at Cala del Vino-northern Porticciolo gulf area. Note the stereoplot where the restoration of the faults with respect to the compressive deformation is reported, showing an original dipping towards the south of these faults. (c) Perspective view of the Digital Outcrop Model where the low-angle angular unconformity and the sinistral transtensive faults are shown. In (c) a detail of a detected transtensional duplex is shown.

same tectonic contact is less clear where it juxtaposes the very-fine deposits of the CVI against the claystone/siltstone of the CDV (Fig. 10b).

Furthermore, the hanging wall of the sinistral fault is affected by a couple of antithetic faults striking approximately WNW-ESE, generating a small graben. The kinematics of these two faults, however, remain unclear due to the absence of slickensides; they could be interpreted as antithetic R' Riedel shears, confined to the hanging wall block of the main left-lateral transtension.

In this sector, an ESE-dipping fault (25N/60°) is present, downthrowing the CVI_a and CVI_b deposits on the conglomerate of CPO_a (Fig. 10c; see also geological cross section F-F' in Fig. 2 and S1). This fault is sealed by the Pleistocene deposits of the Portovesme synthem and is itself cut across by NW-striking normal faults, dipping towards NE at about 55° (see geological cross section F-F' in Fig. 2 and S1).

- Torre del Porticciolo promontory

The promontory of Torre del Porticciolo exposes the Permian sandstone and siltstone of CDV containing vertebrate fossils, overlain by the coarse-grained facies of Porticciolo conglomerate. The entire succession dips towards the NW, with dip angles ranging from 10° to 40° as one moves westwards (Fig. 11a).

This sector of the study area is also characterised by peculiar and spectacular faults. A set of synthetic and antithetic, both left- and right-lateral, NE-striking transtensive faults produces negative flower structures (Fig. 11a-b, e). Mesoscopic strike-slip duplexes are associated with these oblique slip faults. Locally, rotational movements of the fault blocks produce older-on-younger reverse relationships. This transtensional fault system represents the southernmost continuation of the northern Porticciolo gulf-Cala del Vino left-lateral transtensional system.

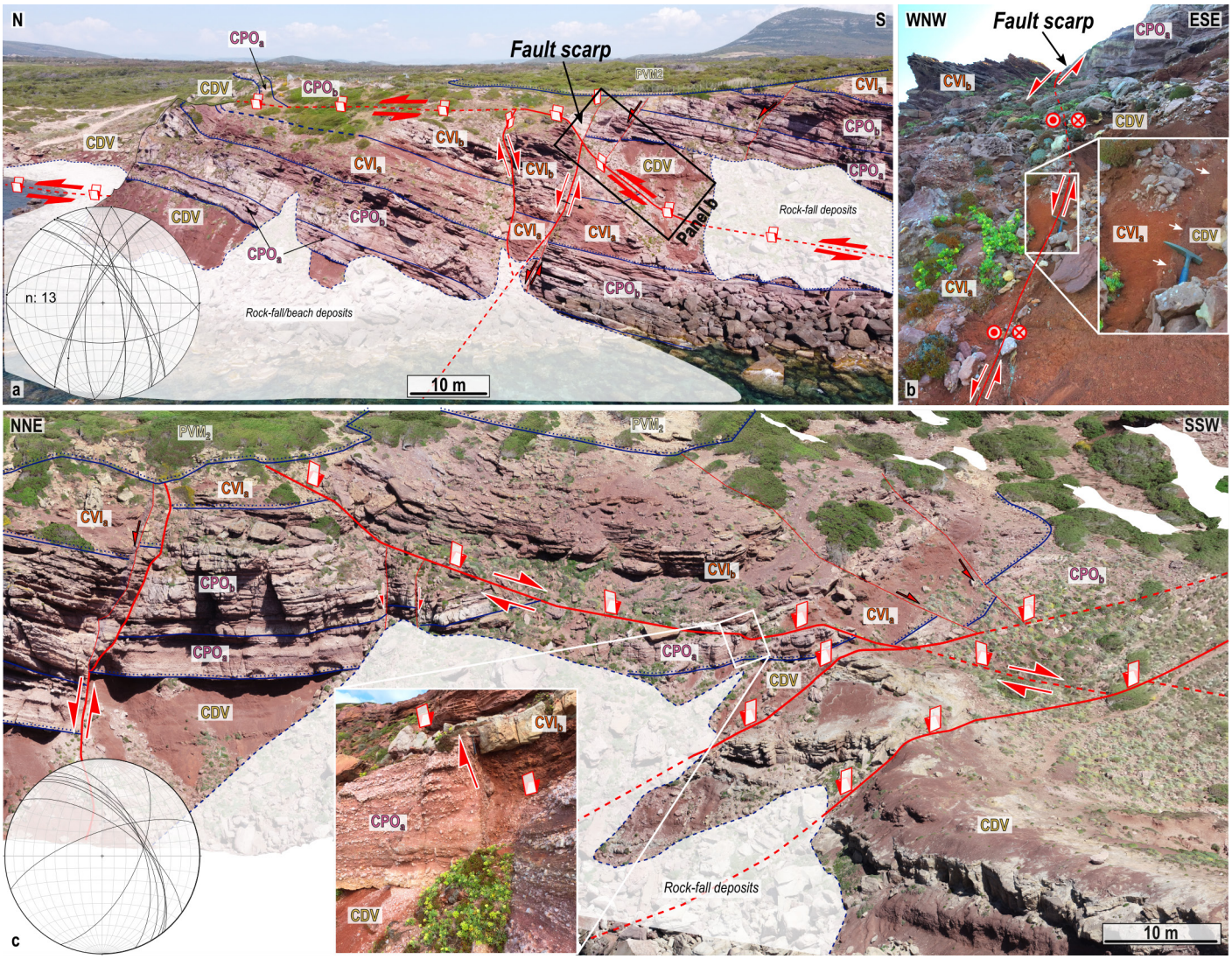

Fig. 10 - (a) Interpreted aerial photographs showing the main tectono-stratigraphic features of the northern part of Torre del Porticciolo cliff. (b) Details of the slip surface of the main high-angle left-lateral transtensive fault that show how the fault surface is less clear where it juxtaposes the very-fine deposits of CVI on the claystones/siltstones of CDV. (c) Interpreted perspective view of the Digital Outcrop Model representing the southern part of the Torre del Porticciolo cliff, where the ESE-dipping fault (25N/60°) downthrowing the CVI$_a$ and CVI$_b$ deposits on the conglomerates of CPO$_a$ also occurs. This sector is dissected by NW-striking normal faults.

The oblique slip lineament is dissected by low-angle compressive, NNE-striking and WNW-dipping faults, although they exhibit limited displacement (up to 1,5 m – Fig. 11a-d). Dip angles range from 22° to 38° and slickenlines on calcite slickensides indicate a dip-slip kinematics (pitch angle of about 80-100°), indicating a top-to-ESE sense of shear. Sigmoidal lenses with dip azimuth towards NW of 45° confirm a top-to-ESE reverse sense of shear. Reverse faults cut the inherited transtensional, mineralised, discrete fault planes, leading to their drag folding consistently with the kinematics of the thrusts (Fig. 11a-c). Associated with this compressive deformation is the development of the NNE-SSW oriented folds exposed between the Torre del Porticciolo promontory and the cliff. Specifically, an open anticline (see the geological cross section F-F' in Fig. 2 and S1) and a tight syncline with a fold plane dipping towards ESE of ~ 45° occur. To date, this syncline is displaced by NE-dipping normal faults, and it is at the footwall of the ESE-dipping fault exposed in the Torre del Porticciolo cliff, which downthrows CVI$_a$ on CPO$_a$.

- Southern Porticciolo gulf

An interesting tectonic feature is exposed in the southern Porticciolo gulf. Discrete and mineralised fault planes cut through the fluvial sandstones and alluvial plain mudstones of CDV (Fig. 11f-g; refer to also geological cross sections D-D' and E-E' in Fig. 2 and S1). This fault system is characterised by high-angle faults with NNE-striking and WNW-dipping direction (dip angles ranging from 45 to 75°). The slickensided faults exhibit kinematic indicators with pitches of 105-125°, indicating a reverse and left-lateral kinematics (Fig. 11g). Sigmoidal lenses and S-C tectonites are also associated with these faults. Locally, drag folds with axial planes dipping towards NW of 45° appear in thin alternations of siltstone and sandstone (Fig. 11f).

Ductile deformation was also identified at the footwall of the left reverse fault, where an asymmetric syncline with an orientation sub-parallel to that of the compressive fault and vergence towards SSE occurs. This fold can be genetically associated with the same

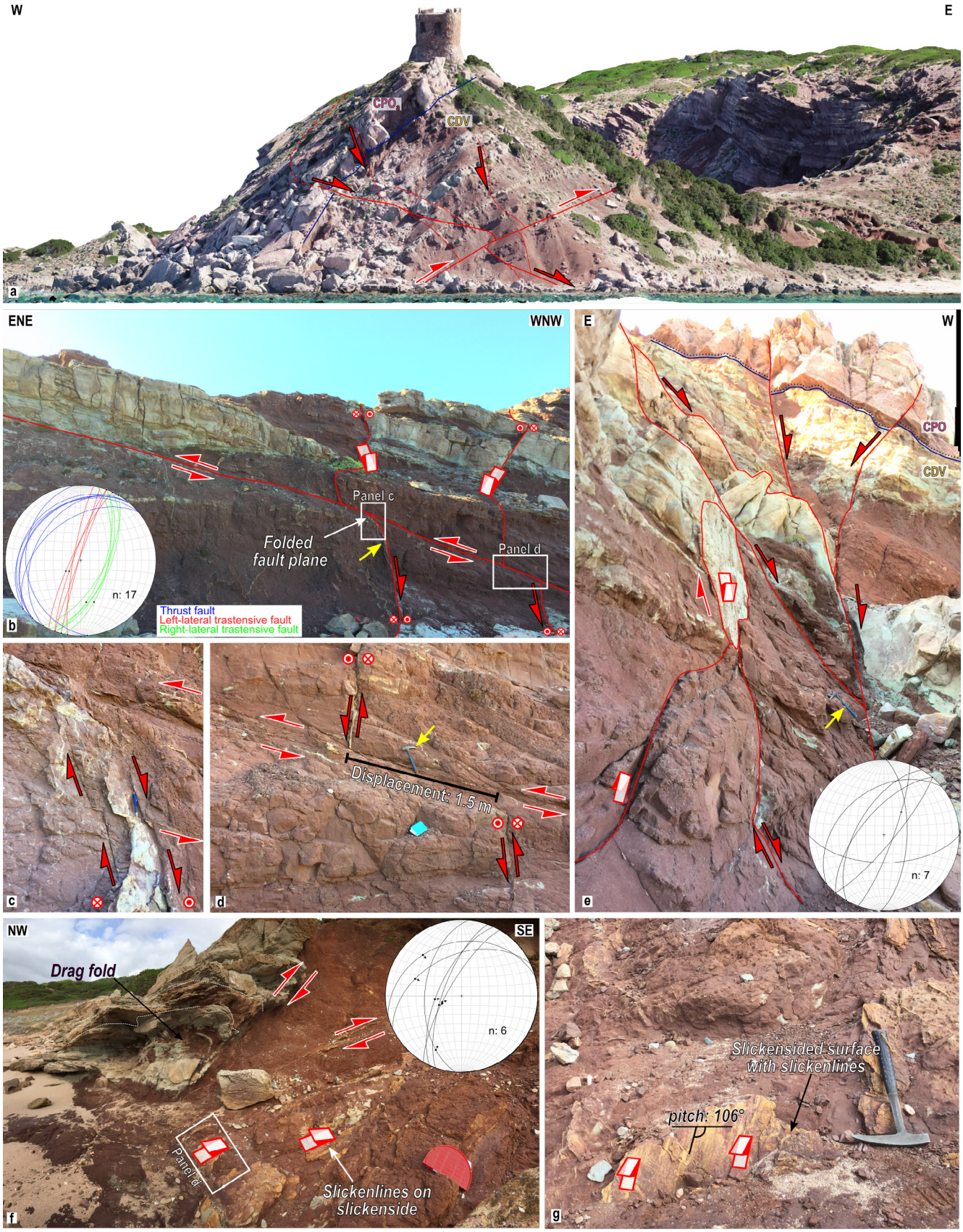

Fig. 11 - (a) Interpreted horizontal-view towards N of the Digital Outcrop Model representing the Torre del Porticciolo promontory. Note the conjugated transtensional faults (red arrows with black contours) displaced and folded by the compressive, SE-verging thrust fault (red arrows with white contours). (b) Field view of the northern slopes of Torre del Porticciolo, where the WNW-dipping thrust showing top-to-ESE sense of shear dissects high-angle, conjugated transtensional faults. (c) Detail of the thrust zone in panel b dissecting and folding previous right-lateral transtensive shear planes. (d) Detail of the thrust zone in panel b showing the 1.5 m-displacement. (e) Negative flower structure associated to the left-lateral transtensive fault system of Torre del Porticciolo. (f) Picture of the compressive shear zone at southern Porticciolo gulf, where a left-lateral transpressive fault system occurs. Note the mesoscopic and localised hanging wall anticline affecting the alternation of clayey and sandy facies of CDV. (g) Detail of a slickensided fault plane showing kinematic indicators. The yellow arrow in panels indicates the hammer as a scale.

shortening phase that led to the development of the high-angle transpressive fault.

- Northern Cala Viola

Along the cliff of northern Cala Viola, a 200 m-wide deformative zone affecting the succession from CDV to CVI_c is exposed (Fig. 12). The most prominent deformations are related to compressive faults (and associated folds), forming an imbricate thrust system (Fig. 12a).

The discrete fault planes trend NNE to ENE and dip towards SE with angles ranging between 20° and 45° (Fig. 12b). Dip-slip kinematic indicators suggest a top-to-NW sense of reverse shear. This sense of shear is supported by the presence of S-C/C' tectonites, sigmoidal lenses and drag folds with axial planes dipping towards 150N/46°. Locally, slickensides of minor splays show slickenlines with pitches of 135°, indicating localised right-lateral movements. These thrust faults displace the succession of at least 15-20 m (see geological cross section B-B' in Fig. 2 and S1), and most of the deformation is accommodated by decametric anticlines and synclines. These asymmetric folds exhibit recumbent to overturned forelimbs, and their axial planes (consistent with the attitude of drag folds) indicate a NW-wards vergence, confirming the SE-NW orientation of shortening (Fig. 12a, e). Associated with deformations bearing northern vergence are thrust planes and folds showing a top-to-SE sense of shear (see Fig. 13c). Such shortening structures suggest back-thrusting and occur in the northernmost part of the study sector, at the hanging wall of a main normal fault (described below).

Folds and thrusts are cut across and downthrown by a complex set of normal faults, mainly dipping towards ENE and SSE with angles

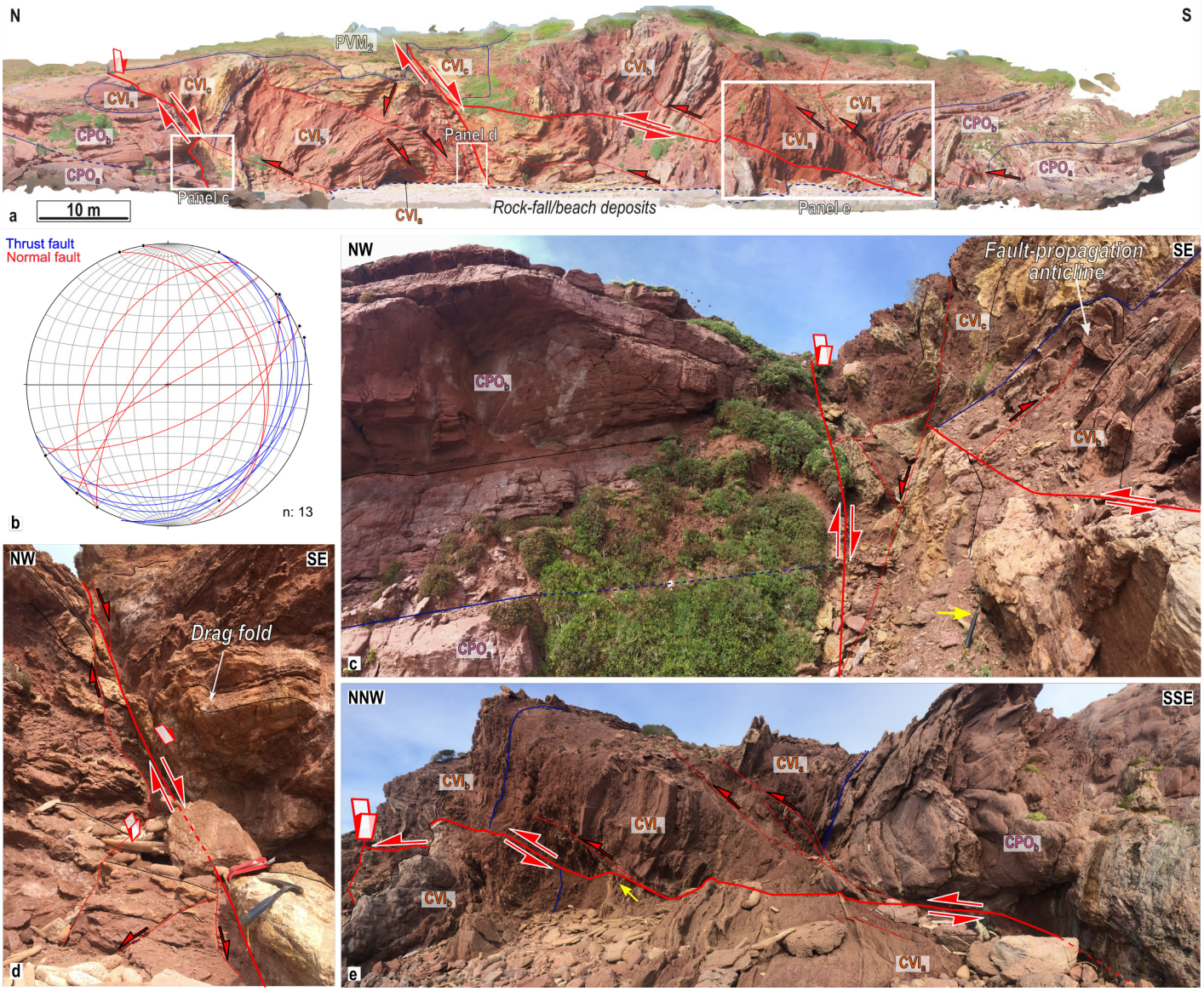

Fig. 12 - (a) Interpreted DOM view of the northern Cala Viola. Here, a compressive deformation zone dissected by normal faults is spectacularly exposed. (b) Stereoplot showing the faults direction of the study sector. (c) Interpreted field picture of the northern, SSE-dipping normal fault bounding and downthrowing the shortening shear zone on a sub-horizontally arranged footwall. Note the occurrence of back-verging (top-to-SE) anticlines and faults in the hanging wall block. (d) SSE-dipping normal fault associated with conjugated, antithetic faults and drag folds. (e) Field view of the thrust zone up-throwing the coarse-grained deposits of Porticciolo conglomerate on the sandy-silty facies of Cala Viola sandstones. Note the small-scale splays associated with the main thrust fault. The yellow arrow in the panels indicates the hammer as a scale.

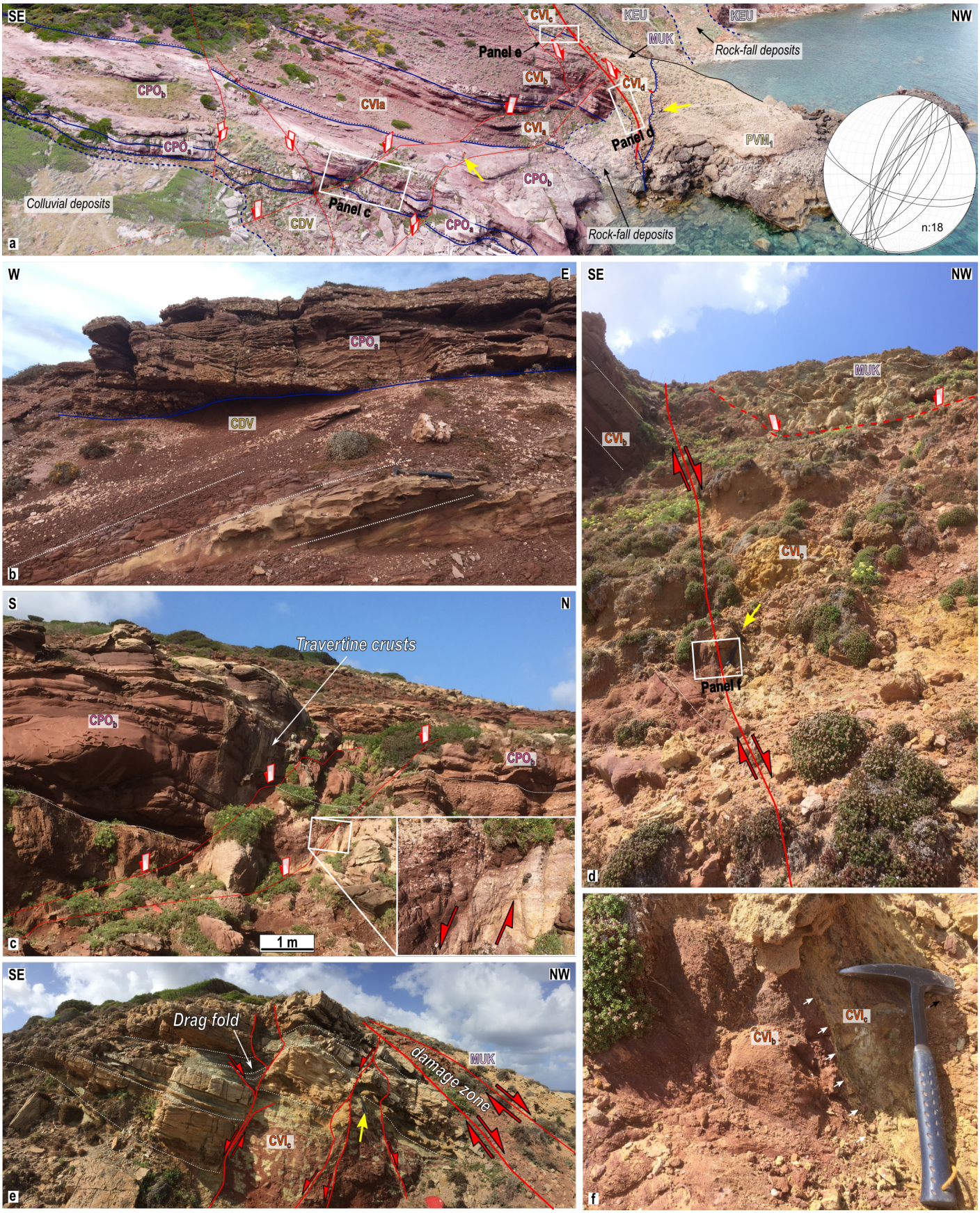

Fig. 13 - (a) UAV-view and interpretation of the southern Cala Viola sector. Yellow arrows indicate geologists as scale. (b) Detail of the angular unconformity between CDV and the overlying CPO$_a$. (c) Field view of the metre-scale SSW-dipping normal fault downthrowing CPO$_b$ on CPO$_a$ deposits. Associated is a detail of the fault zone. (d) Exposure of the dextral normal fault juxtaposing CVI$_c$ on CVI$_b$. The yellow arrow indicates the hammer as a scale. (e) Conjugated faults at the footwall of the main structure shown in panel (d), dissecting CIV$_c$ facies. Associated are drag folds affecting the shaly deposits interbedded in the sandstones. The yellow arrow indicates the hammer as a scale. (f) Detail of the panel (d), where the fault coincides with a marked facies change and is highlighted by the white arrows.

ranging from 35 to 70° (see Fig. 12b-d). The master extensional structures produce up to 30 cm-wide deformation zones and are associated with conjugated sets of faults (Fig. 12c-d). Deflection of beds in proximity to the shear zones is also observed (Fig. 12d), as well as centimetric extensional duplexes.

The northern normal fault bounds the highly deformed compressive zone, displacing it on a sub-horizontally arranged footwall made of the coarse-grained deposits of Porticciolo conglomerate.

- Southern Cala Viola

At Cala Viola, located in the southernmost part of the study area, the entire mapped Permian-Triassic/Jurassic? succession is exposed, although the thickness of CPO_a is reduced (Fig. 13a).

The stratigraphic record is visible at the core of an open anticline trending WNW-ESE and plunging towards the NW at approximately 10°. Similar to the northern Porticciolo gulf, the toplap between CDV and CPO_a is evident and coincides with an angular unconformity of about 10-15° (Fig. 13b). The Permian and Triassic rocks are affected by a series of normal and transtensive faults trending N-S, WNW-ESE and NE-SW. In particular, the top of MUK is juxtaposed against the base of the CVI_c through a sub-vertical tectonic element, the kinematics of which could not be determined (Fig. 13a, d). This element is displaced by a set of NE-striking conjugated faults, causing the downthrowing of the Middle-Upper Triassic deposits (and their structural inheritance) onto the Lower Triassic Porticciolo conglomerate (Fig. 13a, d).

The main, NW-dipping fault is associated with a 10-m wide damage zone (Fig. 13d, e), but localised discrete fault planes were also identified (Fig. 13f). Despite the lack of clear kinematic indicators, the right-lateral transtensive kinematics of this fault was inferred based on the stratigraphic and geometric relationships between the displaced elements. In addition, a net slip of about 25 metres was estimated (see geological cross section A-A' in Fig. 2 and S1). Metre-scale antithetic, SE-dipping faults at the footwall of the main fault produce characteristic domino-like geometries of the faulted blocks and are accompanied by drag folding, especially in the marly facies of CVI_c (Fig. 13e).

Companions of the dominant NE-oriented faults are sub-orthogonal, ESE-oriented and SSW-dipping normal faults, producing up to 2 metres of total displacement (Fig. 13e). These smaller and metre-scale elements appear to be confined to the main NW-dipping transtensive fault shown in figure 13a, d-f, suggesting a tectonic activity related to the main fault. Consequently, these small-scale orthogonal faults likely represent R' Riedel shear faults associated to the NE-trending faults. Travertine patches encrust the hanging wall block of one of these subsidiary faults, as also reported by Casini et al. (2020 in Fig. 6a, c).

Structural stations

During mapping, we detected and digitised 78 fault segments. The resulting fault dataset reveals six sets of fault trends, as depicted in the roseplot (Fig. 14a). In conjunction with field mapping, we also analysed DOMs and identified an additional 384 fault segments (Fig. 14b). These latter fault segments are small-scale structures characterised by limited displacements, usually decimetric, which were not mapped and mappable in the field. We recognised these faults on DOMs, and it was made possible by observing offsets and/or interruptions of the stratigraphic succession. However, due to the resolution limitations of the DOMs, it was not possible to determine the kinematics of these faults.

Based on the stratigraphic separation, we divided the fault dataset in two groups: 258 faults with normal stratigraphic separation, associated with normal and/or transtensive faults (Fig. 14c), and 95 faults with inverse stratigraphic separation, associated with reverse/thrust and/or transpressive faults (Fig. 14d). The later kinematics of potential oblique-slip faults (left- or right-lateral oblique-slip) could not be clearly determined. In addition, for 31 faults, the sense of stratigraphic separation could not be clearly determined.

The statistical analysis of DOM-based fault dataset allowed us to identify six main fault sets, some of which can be subdivided in subsets (Fig. 14b). The analysis of the stereoplots clearly reveals that faults with normal stratigraphic separation (Fig. 14c) display strikes referable to all the identified sets (Fig. 14b). Conversely, the stereoplot of the faults with inverse stratigraphic separation (Fig. 14d) does not display sets 4, 5 and 6, which correspond to W-E, WNW-ENE and NNW-SSE strikes, respectively. Moreover, the latter stereoplot shows two sets of low angle faults dipping about 6° to 36° toward NE to SE (Fig. 14d), which were not previously detected by the Fisher's concentration statistical analysis of the entire dataset (Fig. 14b).

The fault analysis based on the geological map- and DOM-scale structures (Fig. 14) was improved by conducting different high-detail structural stations at the most representative outcrops (described in section 4.2.1). This approach allowed us not only to understand the geometry of the fault network but also determine the fault kinematics (Fig. 15).

At "Cala del Vino'' outcrop (Fig. 15a) three distinguishable sets of faults were observed. The first two sets are represented by N-S trending and W-dipping transtensive faults (dip azimuth/dip 293N/75° and 255N/62°), indicating an extensional regime with a pseudo-horizontal NW-SE trending extension axis. The third set is represented by a NE-SW trending and NW-dipping sinistral transpressive fault (dip azimuth/dip 310N/75°), indicating a mainly transpressive regime with a NNW-SSE trending and NW dipping shortening axis. In addition, the presence of rotated normal faults, originally dipping towards S by about 50°, suggests the existence of a (palaeo-)σ_3 oriented approximately N-S (in present day coordinates).

The outcrops "northern Porticciolo gulf" (Fig. 15b), "Torre del Porticciolo cliff" and "Torre del Porticciolo promontory" (Fig. 15c) exhibit several sets of faults. The main set consists of NNE-SSW and NE-SW trending, near subvertical left-lateral transtensive faults, indicating a mainly extensional regime with a WNW-ESE extension axis. Associated with these faults is a pair of sets of conjugate faults, with NNE-SSW trending and WNW-dipping dextral transtensive faults and ESE-dipping normal faults, respectively, sharing the same axis of extension (palaeo-σ_3 oriented ca. WNW-ESE). Another set comprises ENE-WSW trending and subvertical strike-slip faults, representing a sinistral transcurrent fault system with a main horizontal compression axis oriented about NE-SW. At the "Torre

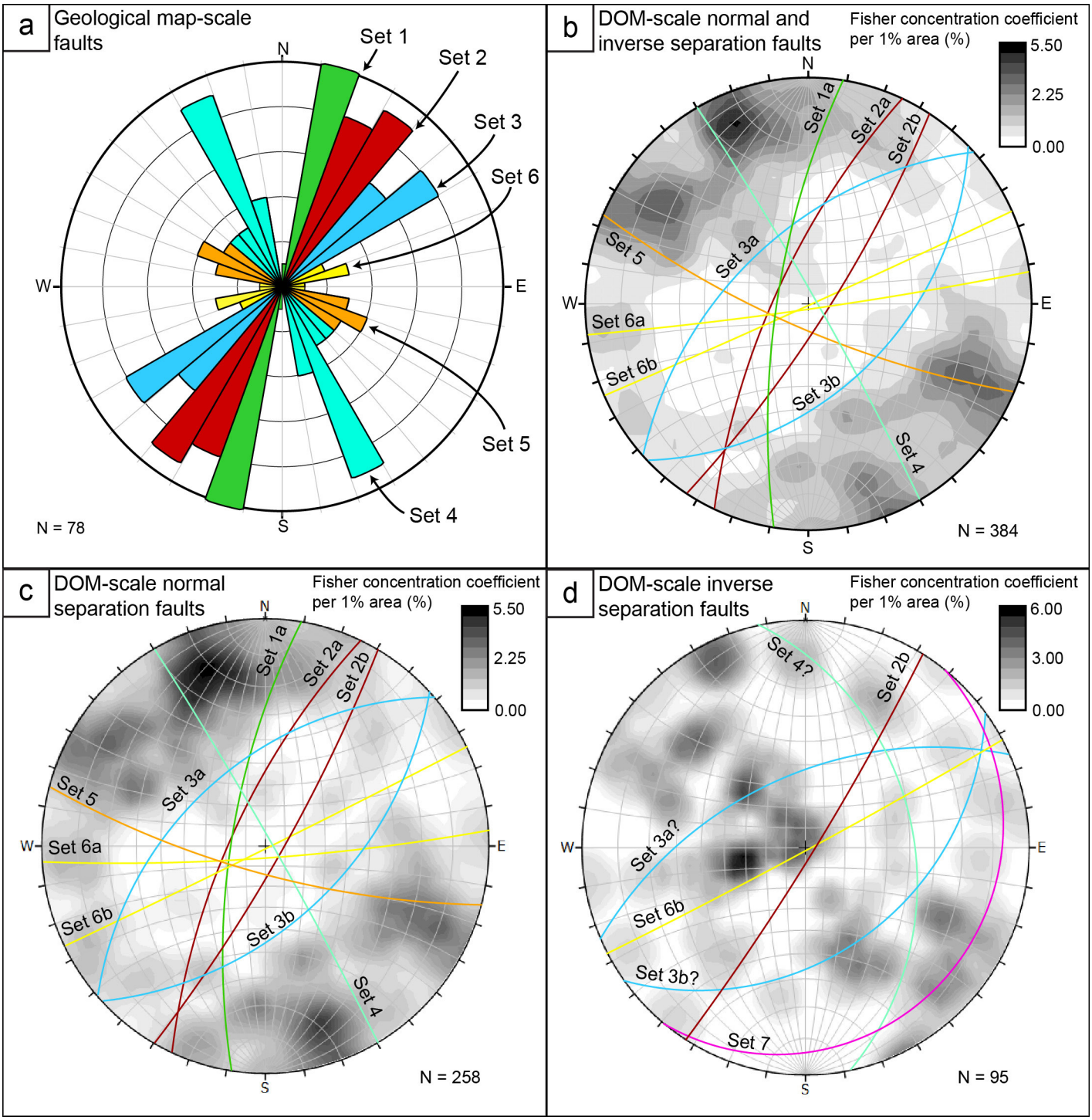

Fig. 14 - (a) Roseplot showing the fault direction detected and digitised at the geological mapping scale where the different sets are represented by different colours. Stereoplots (lower hemisphere, equal angle projection, contour plot per 1% area) of the fault planes mapped on the DOMs, where the mean planes of the fault sets are marked by different colours, representing (b) the entire fault dataset, (c) the normal-separation faults and (d) inverse-separation faults. Note that normal- and inverse-separation faults do not mean normal and inverse faults.

del Porticciolo promontory", another set of NE-SW trending and subvertical sinistral transpressive faults (dip azimuth/dip 92N/65°) is indicative of a mainly compressive regime with a WNW-ESE shortening axis. This fault set is associated with another important set of NW-dipping thrusts (dip azimuth 293N/31° on average) representing a compressive regime with a NW-SE shortening axis. The sixth set consists of WSW-dipping normal faults, indicating an extension regime with a ENE-WSW oriented axis.

At southern Porticciolo gulf (Fig. 15d), three sets of faults were identified. The first set comprises two E-dipping normal faults (mean dip azimuth/dip 104N/35) representing an extension axis mainly oriented NE-SW. Conjugate to these are WSW-dipping normal faults sharing the same extension axis. Another set consists of NNE-SSW and ENE-WSW trending and NW-dipping right-lateral transpressive faults (dip azimuth/dip 310N/55° on average), indicating a mostly compressive regime with a sub-horizontal σ_1 oriented approximately NW-SE.

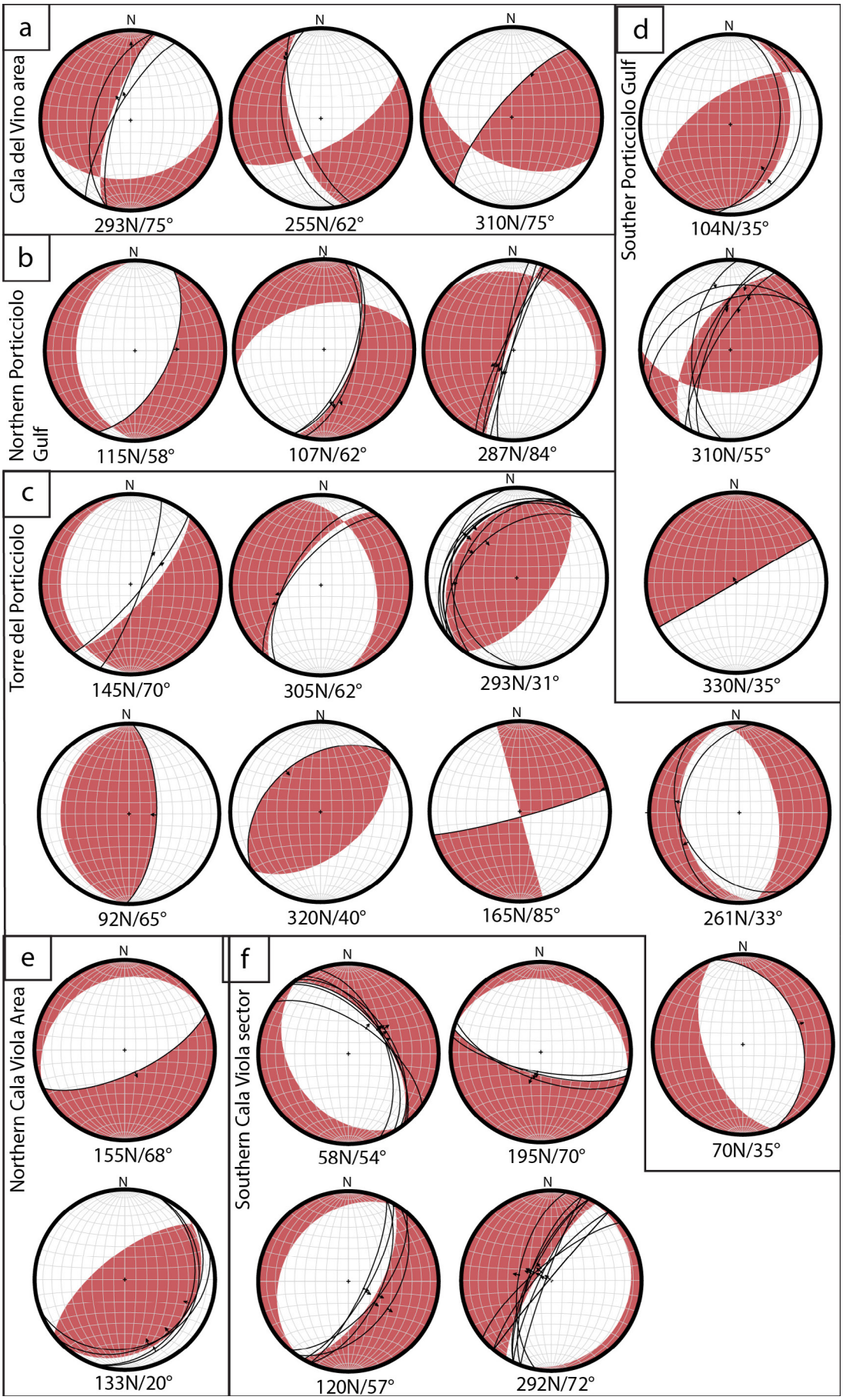

Fig. 15 - (a-f) Lower hemisphere and equal area projection of the fault planes and slip vectors and P-T dihedra (red and transparent areas indicate the extensional and shortening domains) for each fault set detected in the different areas during the detailed structural survey. The P-T dihedra were calculated using Faultkin v.8.1.

At northern Cala Viola (Fig. 15e), two sets of faults are distinguishable. The first set comprises SE-dipping normal faults (dip azimuth/dip 155N/68°), indicating an extensional regime with an NW-SE trending axis. The second set consists of SE-dipping compressive faults (dip azimuth/dip 133N/22° on average) representing an NW-SE shortening axis.

The fault dataset of southern Cala Viola (Fig. 15f) reveals five set of faults. Two sets are composed of NE- and SW-dipping normal faults, compatible with a NE-SW extensional regime. Another pair of sets consists of SE- and NW-dipping right normal faults, indicating an extensional regime with N-S axis. A last set comprises a N-S oriented and W-dipping steep fault represents the last set and coincides with an extension axis oriented approximately E-W.

INTERPRETATIONS: CROSS-CUTTING RELATIONSHIP AND RELATIVE TIMING OF DEFORMATION STRUCTURES

The analysis of cross-cutting relationships of the deformation structures observed and mapped in the area allow us to interpret the relative timing of these tectonic elements.

At Cala Viola (Fig. 13; see geological cross section A-A' in Fig. 2 and S1) and northern Porticciolo gulf (Fig. 9; see geological cross section I-I' in Fig. 2 and S1), one of the earliest deformation structures detected in the study area is visible. This structure is represented by the tilting of middle Permian deposits of CDV, reaching angles of 15-20°. The timing of this tilting can be constrained, providing a minimum age for its occurrence. Specifically, the deformation postdates the deposition of the upper part of CDV and predates the erosional phase that resulted in the unconformity where the coarse-grained facies of CPO_a rest. Consequently, this phase of tectonic instability can be confined to a time interval between the Roadian and the Induan. Since the Triassic peneplanation confines the tilting, and both the Lower Mesozoic erosional unconformity and the underlying Permian deposits are cut by younger deformations, we can confidently assert that this deformative phase is the oldest one identified in the study area.

In the Cala del Vino-Torre del Porticciolo area, we observe other cross-cutting relationships that help us to understand the relative timing of the detected deformation structures. Here, the "low-angle" normal fault (referred to as "palaeofault" in Figs. 2, 9 and S1), which is involved in the hanging wall anticline of a high-angle and right-lateral transpressive fault striking ENE-WSW, is displaced by the transpressive structure (see geological cross section I-I' in Fig. 2 and S1). This NNW-SSE shortening phase caused the deformation and rotation of the originally S-dipping extensional plane, as evidenced by restoring to the horizontal the bed attitude of the Permian deposits dissected by such lineament (see Fig. 9a). The set of synforms and antiforms, striking about ESE-WNW and associated to the right-lateral compressive lineament, is then cut and displaced by a set of NNE-striking and WNW-dipping left-lateral transtensive faults.

At the Torre del Porticciolo-Cala del Vino, the left-lateral transtensional faults are displaced by thrusts with a top-to-ESE sense of shear (see geological cross section F-F' in Fig. 2 and S1, and Fig. 11), and they are also rotated by the development of the Torre del Porticciolo ~N-S striking anticline, consistent with the same NW-SE compressive deformation. The same oblique slip faults are dissected by NW-striking conjugated normal faults (see Figs. 2 and 10).

At northern Cala Viola, a series of compressive structures, represented by NNW-verging imbricated thrusts and associated recumbent to overturned NW-verging folds, are displaced by ENE- to NNE-trending and approximately SE-dipping extensional faults (see geological cross section B-B' in Fig. 2 and S1, and Fig. 12).

In the southern part of the Cala Viola, the sub-vertical fault juxtaposing the top of MUK on the base of CVI_c is dislocated by a SW-NE oriented right-lateral transtensional fault system.

DISCUSSIONS

Need for a revision of the "classical" Triassic stratigraphy of Northern Sardinia

The detailed geological mapping of the Permian and Triassic continental deposits in the Nurra region, based on a pure lithostratigraphic approach, allows to identify a still open problem, especially for the Lower Mesozoic deposits. Even though the Lower-Middle *p.p.* Triassic continental successions of Sardinia were assigned by the *Commissione Italiana di Stratigrafia* (Italian Commission on Stratigraphy - hereafter, CIS) to the Buntsandstein as a formation-rank unit (Gandin et al., 2007), in this work we show that not only the Triassic continental facies can be mapped as distinct units, but also that the same deposits can be further subdivided into lithofacies. In agreement with the subdivision made by Cassinis et al. (2002, 2003), in this work, we consider the Porticciolo conglomerate and the Cala Viola sandstones as distinguishable and mappable formations. The latter in analogy with the French lithostratigraphy, where the Triassic continental deposits of Provence, that were palaeogeographically contiguous to the study ones prior to the Sardinia-Corsica rotation, are grouped in *Poudingue de Port-Issol* and *Grès de Gonfaron* formations (equivalents of Porticciolo conglomerate and Cala Viola sandstones, respectively – Cassinis et al., 2003; Durand, 2006, 2008). Furthermore, in the Germanic basin comparable deposits are referred to the Buntsandstein Group (Bachmann & Kozur, 2004; Kozur & Bachmann, 2005), in turn subdivided in sub-groups and formations. As a consequence, and in good agreement with the lithostratigraphy of the classical localities for the continental Triassic deposits, it would be necessary to review the lithostratigraphy of Sardinia, suggesting that the lithostratigraphic nomenclature (i.e., Buntsandstein) can be preserved but the rank of the unit should be changed from formation to group. In turn, we do not agree with the nomenclature proposed by other authors (Costamagna & Barca, 2002; Costamagna, 2012), who propose the improper name Verrucano Sardo (introduced by Vardabasso, 1966 only for the basal conglomerates of the "Permotriassic" succession and later used for the entire "Permotriassic" succession by Gasperi & Gelmini, 1979) as a formational name encompassing the Porticciolo conglomerate and the Cala Viola sandstones.

A complete redescription of the Triassic stratigraphic units shown in the map of this study is in progress, along with a detailed

facies analysis of key stratigraphic sections of the Porticciolo conglomerate and Cala Viola sandstones formations, to correctly formalise these units with CIS standards. In sub-chapters 4.1.2 and 4.1.3 the proposed stratigraphic revision is explained.

How many deformations episodes?

The results of fault analysis performed at various scales, including the geological mapping (Fig. 14a), the DOMs (Fig. 14b-d) and the detailed structural stations (Fig. 15), reveal a complex tectonic history of the study area, characterised by different tectonic regimes. The general DOM analysis (Fig. 14) indicates that certain sets of faults (e.g., Sets 2b, 3 and 6b) can exhibit both normal and inverse stratigraphic separation, whereas the detailed structural analysis (Fig. 15) shows how they can display different kinematics. For instance, faults of Set 2 display different preferential kinematics: right transtensive at Cala del Vino area, left strike slip at northern Porticciolo gulf area, left transpressive at southern Porticciolo gulf area, and normal dip-slip at southern Cala Viola area. Moreover, the examination of the structural data from individual outcrops (Fig. 15) reveals the occurrence of different deformation events with various extension and/or shortening axes.

By combining the results of the geological mapping and the DOMs analysis (Fig. 14) with the results of the detailed structural stations (Fig. 15), we can depict a complex tectonic history. This history indicates that some of the investigated fault sets could have experienced different tectonics regimes, as follows:

- Faults of set 1 mainly underwent an extensional regime with a E-W extension axis;
- Faults of set 2 experienced a sinistral transpressive regime with a NW-SE shortening axis, but also an extensional tectonic with a WNW-ESE extension axis;
- Faults of set 3 mainly underwent an extensional regime with a NW-SE extension axis;
- Faults of set 4 mainly underwent an extensional regime with an ENE-WSW extension axis;
- Faults of set 5 mainly underwent an extensional regime with a NE-SW extension axis, but two transpressive regime with WNW-ESE and NW-SE shortening axis;
- Faults of set 6 experienced an extensional regime with a NNW-SSE extension axis, and two transpressive regimes with NE-SW and NW-SE shortening axis.

Previous studies by various authors (Cassinis et al., 1980; Cherchi & Trémolières, 1984; Fanucci et al., 2001; Ziegler & Stampfli, 2001; Carmignani et al., 2001, 2004; Zattin et al., 2008; Oggiano et al., 2018; Casini et al., 2020) proposed that NW Sardinia has been exposed to different tectonic events from the Ordovician to the Holocene. To simplify the comprehension of the tectonic reconstruction presented here, the tectonic events reported in literature are named and contextualised as follow:

- Event 1, an extensional event related to the Permian-Triassic intracontinental rifting resulting from the collapse of the Variscan orogeny;
- Event 2, an extensional phase related to the Jurassic rifting of the Ligurian-Piedmont Ocean (Bajocian – Bathonian), leading to the development of a wide, subsident shallow water carbonate platform with internal stratigraphic-structural heterogeneities;
- Event 3, a NNW-SSE oriented extensional event of latest Early Cretaceous (Aptian-Albian) age, characterised by a ENE-WSW normal faulting. This phase, known as "Austrian phase" *Auct*., is represented by extensive angular unconformities/hiatuses in carbonate platform settings and is related to far field deformations of the Pyrenaic accretionary wedge;
- Event 4, a NNW-SSE transpressive and compressive event of Late Cretaceous age, characterised by NNE-SSW left-lateral strike slip faults, related NNW-SSE trending open folds, and NE-SW trending normal faults (e.g., pull-apart basins). Pieces of evidence of this deformation phase, known as "Laramian" tectonics, are reported by Oggiano et al. (2018) in the neighbouring Sassari area and are represented by faults (e.g., Nalvonazzos fault) and folds;
- Event 5, in turn subdivided in two deformative sub-events: Event 5a is a NW-SE oriented compressive event of Eocene age, and Event 5b is a NE-SW transcurrent event of Oligocene-earliest Miocene (Aquitanian) age. These deformations are ascribed to the "Pyrenaic phase" and are represented by i) ENE-WSW oriented left-lateral transcurrent faults, ii) NW-SE striking pull-apart/ transtensive basins and minor transpressive structures, and iii) NE-SW trending folds. The combination of these tectonic structures indicates a main NW-SE shortening direction, and field evidence is reported by Oggiano et al. (2018) in the contiguous sector of Sassari (e.g., Campanedda anticline, Serralonga syncline), and by Carmignani et al. (1992 - Mt. Albo fault, Chilovani-Birchidda basin).
- Event 6, a NNE-SSW extensional event of Burdigalian age, represented by the NNW-SSE trending normal faults, and conjugate E-W and WNW-ESE trending normal faults, related to the opening of the Balearic basin and to the counterclockwise rotation of the Sardinia-Corsica block. This normal faulting phase produced the tilting towards NE of the Nurra sector and a characteristic horst and graben/semigraben setting of the western margin of Sardinia;
- Event 7, in turn subdivided in two extensional sub-events: Event 7a, Serravallian in age, represented by E-W trending normal faults and associated with a NNE-SSW trending extension axis, and Event 7b Pliocene in age , characterised by a NW-SE extension axis and represented by N-S and NE-SW trending normal faults. Field evidence of both the deformations are described by Funedda et al. (2000) and Carmignani et al. (2001) in the Sassari sector (Ittiri fault);
- Event 8, Pleistocene-Holocene in age, characterised by NW-SE and NNE-SSW trending normal faults reactivating inherited structures and referable to extension axes oriented NW-SE and NE-SW.

In the following, the main tectonic structures identified in the study area are tentatively referred to the previously described events (Fig. 16).

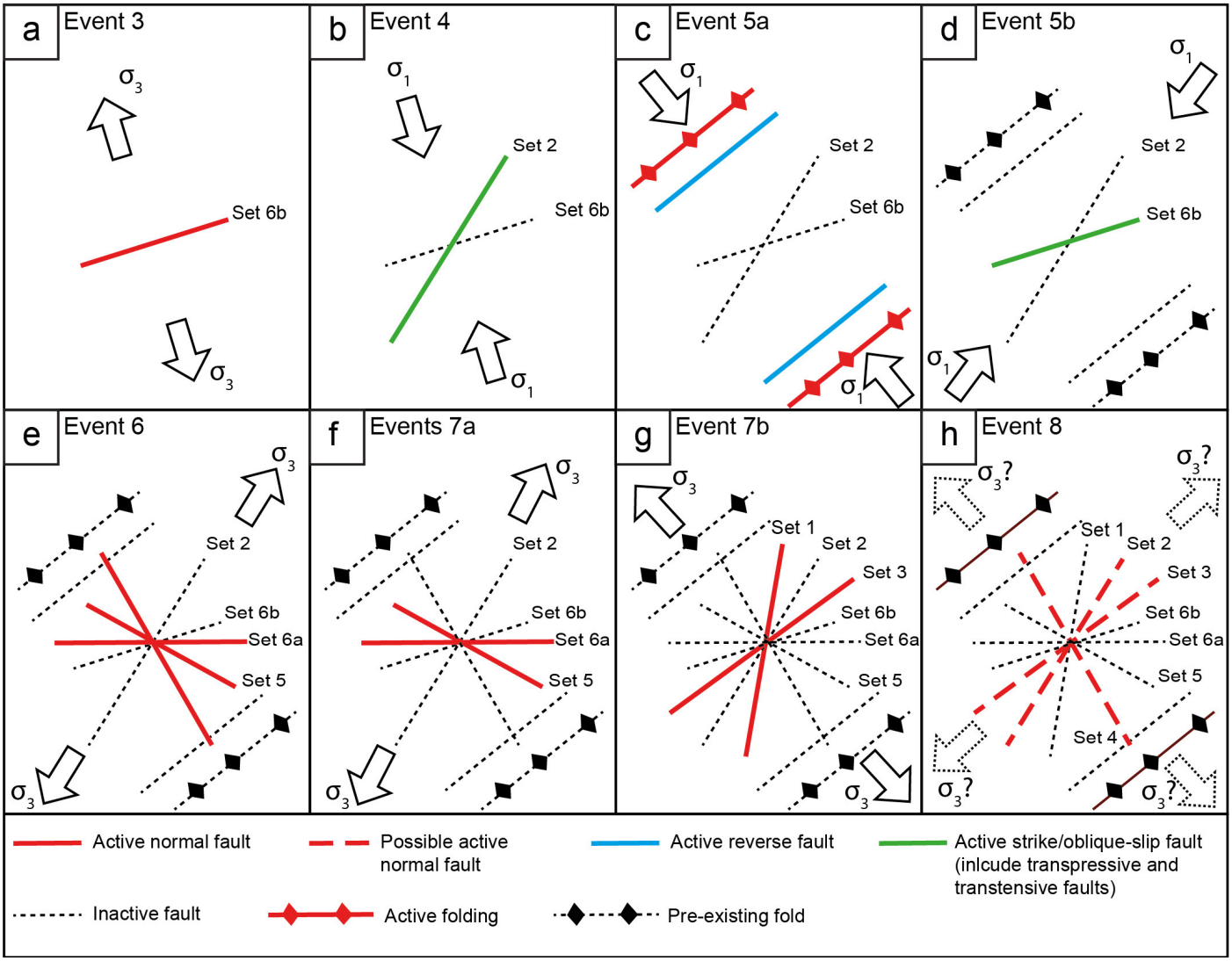

Fig. 16 - Conceptualization of the deformation structures formed or reactivated during the different tectonic events: (a) Event 1 refers to the Aptian-Albian extensional event; (b) Event 4 refers to the Late Cretaceous transpressive and compressive event; (c) Event 5a refers to the compressive event of the Pyrenean phase; (d) Event 5b refers to the transcurrent event of Oligocene-earliest Miocene (Aquitanian) phase; (e) Event 6 refers to the Burdigalian extensional event; (f) Event 7a and (g) Event 7b refer to the two extensional events occurred in the (f) Serravallian and (g) Pliocene; (h) Event 8 refers to two extensional events of Pleistocene-Holocene age.

Indirect evidence of the Event 1, related to the pre-Triassic extensional tectonics, is present in the study area and corresponds to the tilting of Permian deposits of CDV. The bed attitudes of the CDV sandstones and claystones often contrast with those of the coarse-grained facies of Porticciolo conglomerate, forming toplap unconformities with angles reaching 15-20° (Figs. 9 and 13). This unconformable relationship is observed in Cala Viola (Fig. 9 c and 13 b; see also geological cross section A-A' in Fig. 2 and S1) and northern Porticciolo gulf (Fig. 10; see geological cross section I-I' in Fig. 2 and S1), suggesting the occurrence of synsedimentary tectonics predating the erosive phase at the base of Triassic deposits, leading to the folding of Permian strata. Currently, we lack geochronological and regional constraints on this phase, but it should be temporarily located between the early middle Permian and the late Early Triassic.

Event 2 (Jurassic rifting) and Event 3 (Aptian-Albian) have not been clearly identified due to the absence of unequivocal evidence and their possible relation with other structures of NW Sardinia. Notwithstanding, at Cala del Vino, a pre-Late Cretaceous event (pre-Event 4) can be attributed to low angle normal faults (referred to as "palaeofault" in Figs. 2, 9a-b and S1). These normal faults are likely Permian, Triassic, Jurassic and Early Cretaceous in age. Their exact age cannot be determined due to the lack of exposure (and displacement) of deposits younger than the Permian. Nevertheless, a minimum age can be determined by constraining it with the displacement of the oldest mapped deposits and the subsequent reverse/transpressive deformation that have folded and cut through them. The latter compressive deformation is represented by ENE-WSW striking transpressive faults (Fig. 9) and associated WSW-ENE folds, indicating a NNW-SSE shortening direction consistent with Event 4, which is Late Cretaceous in age. These folds are then cut and displaced by the NNE-SSW striking and WNW-dipping left lateral transtensive fault (i.e., Set 2 in Fig. 14). This fault is coherent with the NNE-SSW transpressive event (Event 4) that

occurred in Late Cretaceous and generated NNE-SSW left-lateral transpressive/transtensive faults in the nearby Sassari area, such as the Nalvonazzos and Su Zumbaru faults (Oggiano et al., 2018).

As previously described, at Torre del Porticciolo, the prosecutions of these NNE-SSW striking left-lateral transtensive faults are cut and displaced by low-angle, SE-verging compressive deformation structures, whose strikes are compatible with the trend of Set 3 (Fig. 14). These thrust faults are associated with a series of folds with NE-SW axis indicating a NW-SE shortening direction. This is consistent with the compressive Event 5 attributed to the Pyrenean phase (Cherchi & Tremolies, 1984; Barca & Costamagna, 1997; Carmignani et al., 2001, 2004), which produced several compressive structures in NW Sardinia, including the Campanedda anticline and Serralonga syncline (Oggiano et al., 2018). Compressive structures related to the Event 5 were also identified in the northern Cala Viola area. Here, NW-verging low-angle thrusts and NE-SW folds indicate a NW-SE shortening direction, consistent with the Event 5a. These thrusts are displaced by NNW-SSE and ENE-WSW trending (Set 4 and Set 3, respectively, in Fig. 14) normal faults, which align with the further extensional tectonic events reported in literature. In particular, the NNW-SSE normal faults (i.e., Set 4) align with the kinematics of the Burdigalian extensional phase (Event 6), which caused the deepening towards E of the Porto Torres basin (Oggiano et al., 2018). Conversely, the ENE-WSW trending and SSE-dipping normal faults (i.e., Set 3) cutting across the NW-verging thrust can be associated to the extensional Events 7b (Pliocene) and/or 8 (Pleistocene-Holocene). The Event 7b could have reactivated normal faults with N-S and NE-SW trends or developed new faults with comparable strikes (i.e., Sets 1 and 3 – Fig. 14), consistent to an extension axis oriented NW-SE. The Event 8 may have probably reactivated faults with strikes consistent with the Set 2 (NNE-trending), Set 3 (NE-SW) and Set 4 (NW-striking) (Fig. 14), consistent to two main extension axes oriented NW-SE and NE-SW reported by Casini et al. (2020). The faults exposed at southern Cala Viola, referred to as the Le Bombarde fault by Casini et al. (2020), could be related to this tectonic event. Although Casini et al. (2020) attribute possible Late Pleistocene-Holocene activity to these faults, our field data do not allow us to confirm this interpretation; furthermore, there is no evidence of recent tectonic activity reported in Italian seismic databases (CPTI, DISS, ITHACA).

As mentioned earlier, no clear evidence for the Early Cretaceous (Aptian-Albian) extensional Event 3 is found in the study area. However, looking at the northern Cala Viola area, the normal fault bounding northward the highly-deformed compressive zone indicates a significant change in the deformation style and mechanisms (see section 4.3.1.5 “northern Cala Viola”). The footwall block of the fault is sub-horizontally arranged and displays limited, mainly extensional deformations, whereas the hanging wall is pervasively faulted and folded by shortening stresses verging towards NNW. Back-verging thrusts and folds (i.e., top-to-SE sense of shear) are associated with the main SE-dipping thrusts (see Fig. 12c), displaying limited displacement and localised close to the normal fault (few metres far from the extensional shear plane). In addition, the normal fault has a comparable orientation with the structures referred to the Aptian-Albian Event 3 (i.e., ENE-WSW - Carmignani et al., 2001; Oggiano et al., 2018). Considering these observations , we can speculate that this fault developed during the latest Early Cretaceous, causing the downthrow of the well-bedded sandstones and siltstones of Cala Viola sandstones (hanging wall block) on the massive, coarse-grained deposits of Porticciolo conglomerate (footwall block). The result of this normal faulting was a rheological contrast between the horst-block (mechanically more competent) and the hanging wall succession (prone to host plastic deformations), influencing the development of younger compressive deformations. During the Late Cretaceous, the propagation of NE-SW trending transpressive/compressive structures (Event 4) towards NW was accommodated by the less competent rocks (i.e., Cala Viola sandstones), leading to intense strain consisting of both brittle and plastic deformations. In contrast, the SE-dipping (opposite to the vergence of compression) high-angle normal fault and its footwall acted as a rheological barrier, counteracting the tectonic shortening and producing a buttressing effect. This behaviour resulted in the development of confined back-thrusts and back-verging folds, limited to a belt near the buttress. Furthermore, positive inversion of the hanging wall block along the SE-dipping normal fault, subsequently reactivated as a dip-slip extensional element during younger tectonic phases, cannot be excluded. Successive extensional events (Event 5 and younger) could have overprinted the previously described evidence (e.g., drag fold of Fig. 15d). Unfortunately, the lack of striae on the normal fault-surface prevents us from confirming such interpretation. Similar features have been described by Butler (1989), Dart et al. (1995), Bailey et al. (2002) and Uzkeda et al. (2013).

Regarding Event 5b, there is no clear evidence of deformation, but the presence of ENE-WSW sinistral transcurrent faults between the Torre del Porticciolo cliff and the promontory (Fig. 2) suggests a possible connection with the Oligocene-earliest Miocene (Aquitanian) phase, which formed a series of coherent ENE-WSW trending sinistral strike-slip structures (i.e., Chilivani-Berchidda transtensive basin: Carmignani et al., 1994; Oggiano et al., 1995).

CONCLUSIONS

The detailed geological mapping, incorporating stratigraphic, sedimentological and structural analysis, along with the drone-based aerial photogrammetry, allows us to propose a stratigraphic revision and qualitatively reconstruct the complex tectono-stratigraphic history of the Cala Viola-Cala del Vino area. We demonstrate that the Porticciolo conglomerate and the Cala Viola sandstones can be regarded as two distinct and mappable formations, in analogy to the French lithostratigraphy of the Triassic continental deposits of Provence. In addition, we suggest elevating the lithostratigraphic rank of the Buntsandstein from formation to group, similar to the comparable deposits of the Germanic basin.

Despite the absence of geochronological constraints for the identified structures, such as radiometric dating, the analysis of topology and cross cutting relationship of fault networks has allowed us to attribute these structures to at least eigth different tectonic events. Each event resulted in the formation of discrete

shear zones, accompanied by associated folds, or the reactivation of pre-existing discontinuities. These new data make it possible to reconstruct the complex tectonic history affecting NW Sardinia since the deposition of the middle Permian deposits to the Holocene.

In the future, conducting quantitative analyses of the faults age/timing will provide time constraints, contributing to a more precise reconstruction of the tectonic history of the area and deeper understanding of the plate tectonics/geodynamic of NW-Sardinia.

ELECTRONIC SUPPLEMENTARY MATERIAL

This article contains electronic supplementary material which is available to authorised users. In particular, the detailed geological map and the frame elements are provided as Supplementary Material I (S1). Details on the UAV survey and DOMs, as well as the original field pictures of the plates, are reported in Supplementary Material II (S2).

ACKNOWLEDGEMENTS

The Editor-in-Chief Federico Rossetti, the Associate Editor Giulio Viola, the Guest Editor Simone Fabbi, the reviewers Marc Durand and Andrea Brogi are acknowledged for improving the quality of the manuscript.

Special thanks are due to Cesare Perotti for the financial support of the drone photogrammetric survey and the APCs, and to the Azienda Speciale Parco di Porto Conte for the drone flight permission. We warmly thank all the friends, colleagues and supporters who contribute to the crowdfunding campaign 'Permian Hunters - *Alla scoperta degli antenati dei mammiferi nel Permiano della Sardegna'*, conceived and managed by MR. AR acknowledge also support from PRIN Project DEtailing thE Palaeogeography of Southern PAlaeoeurope by meanS of biosTratigraphic correlation and basin development in the Palaeozoic to early Mesozoic time-frame: case histories from the Italian record (DEEP PAST).

Also, we would like to acknowledge Anna Giamborino, Giulia Innamorati, Simone Maganuco, Fabio Manucci, Eva Sacchi, Costantino Zuccari for their support in the field. AR wish to thank C. Stefani, D.Fontana, M. Durand and the late G. Cassinis and C. Neri for the fruitful discussion in the field during many years of studying the succession.

REFERENCES

Allen J.R.L. (1963) - The classification of cross-stratified units, with notes on their origin. Sedimentology, 2, 93-114.

Allmendinger R.W., Cardozo N. & Fisher D. (2012) - Structural geology algorithms: Vectors and tensors in structural geology: Cambridge University Press, 302 p.

Andreucci S., Pascucci V. & Clemmensen L.B. (2006) - Upper Pleistocene coastal deposits of West Sardinia: a record of sea-level and climate change. GeoActa, 5, 79-96.

Andreucci S., Clemmensen L.B., Murray A.S. & Pascucci V. (2010) - Middle to late Pleistocene coastal deposits of Alghero, northwest Sardinia (Italy): Chronology and evolution. Quatern. Int., 222, 3-16.

Bachmann G.H. & Kozur H.W. (2004) - The Germanic Triassic: correlations with the international chronostratigraphic scale, numerical ages and Milankovitch cyclicity. Hallesches Jahrb. Geowiss., 26, 17-62.

Bachtadse V., Aubele K., Muttoni G., Ronchi A., Kirscher U. & Kent D.V. (2018) - New early Permian paleopoles from Sardinia confirm intra-Pangea mobility. Tectonophysics, 749, 21-34.

Bailey C.M., Giorgis S. & Coiner L. (2002) - Tectonic inversion and basement buttressing: an example from the central Appalachian Blue Ridge province. J. Struct. Geol., 24, 925-936.

Barca S. & Costamagna L.G. (1997) - Compressive ''Alpine'' tectonics in Western Sardinia: geodynamic consequences. C. R. Acad. Sci. IIA, 325(10), 791-797.

Baucon A., Ronchi A., Felletti F. & Neto de Carvalho C. (2014) - Evolution of Crustaceans at the edge of the end-Permian crisis: Ichnonetwork analysis of the fluvial succession of Nurra (Permian-Triassic, Sardinia, Italy). Palaeogeogr. Palaeocl., 410, 74-103.

Borruel-Abadía V., Barrenechea J. F., Galán-Abellán A. B., De la Horra R., López-Gómez J., Ronchi A., Luque F. J., Alonso-Azcárate J. & Arche A. (2019) - Could acidity be the reason behind the Early Triassic biotic crisis on land? Chem. Geol., 515, 77-86.

Bourquin S., Durand M., Diez J.B., Broutin J. & Fluteau F. (2007) - The Permian–Triassic boundary and Early Triassic sedimentation in Western European basins: An overview. J. Iber. Geol., 33, 221-236.

Bourquin S., Bercovici A., López-Gómez J., Diez J.B., Broutin J., Ronchi A., Durand M, Arché A., Linol B. & Amour F. (2011) - The Permian–Triassic transition and the onset of Mesozoic sedimentation at the northwestern peri-Tethyan domain scale: Palaeogeographic maps and geodynamic implications. Palaeogeogr. Palaeocl., 299, 265-280.

Brocklehurst N., Romano M. & Fröbisch J. (2016) - Principal component analysis as an alternative treatment for morphometric characters: phylogeny of caseids as a case study. Palaeontology, 59(6), 877-886.

Butler R.W.H. (1989) - The influence of pre-existing basin structure on thrust system evolution of the Western Alps. In: Cooper M.A. & Williams G.D.(Eds.), Inversion Tectonics. Geol. Soc., London, Spec. Publ., 44, 105-122.

Carmignani L., Carosi R., Disperati L., Funedda A., Musumeci G., Pasci S. & Pertusati P.C. (1992) - Tertiary transpressional tectonics in NE Sardinia. In: Carmignani L. & Sassi F.P. (Eds.), Contributions to the Geology of Italy with special regard to the Paleozoic basements. A volume dedicated to Tommaso Cocozza. IGCP, 276(5), 83-96.

Carmignani L., Oggiano G., Barca S., Conti P., Salvadori I., Eltrudis A., Funedda A. & Pasci S. (2001) - Geologia della Sardegna. Note illustrative della Carta Geologica della Sardegna a scala 1:200.000. Mem. Descr. Carta Geol. d'It., 60, 1-283.

Carmignani L., Barca S., Disperati L., Fantozzi P.L., Funedda A. & Oggiano G. (1994) - Tertiary compression and extension in the Sardinian basement. Boll. Geofis. Teor. Appl., 36(141-144), 45-62.

Carmignani L., Funedda A., Oggiano G. & Pasci S. (2004) - Tectono-sedimentary evolution of southwest Sardinia in the Paleogene: Pyrenaic or Apenninic Dynamic? Geodin. Acta, 17(4), 275-287, https://doi.org/10.3166/ga.17.275-287.

Casini L., Andreucci S., Sechi D., Huang C.Y., Shen C.C. & Pascucci V. (2020) - Luminescence dating of Late Pleistocene faults as evidence of uplift and active tectonics in Sardinia, W Mediterranean. Terra Nova, 32(4), 261-271, https://doi.org/10.1111/ter.12458.

Cassinis G., Elter G., Rau A. & Tongiorgi M. (1980) - Verrucano: tectofacies of the Alpine-Mediterranean southern Europe. Mem. Soc. Geol. It., 20, 135-149.

Cassinis G., Cortesogno L., Gaggero L., Ronchi A. & Valloni R. (1996) - Stratigraphic and petrographic investigations into the Permo-Triassic continental sequences of Nurra (NW Sardinia). Cuad. Geol. Iber., Spec. Issue 21, 149-169.

Cassinis G. & Ronchi A. (2002) - The (late-) Post-Variscan continental succession of Sardinia. Rend. Soc. Paleontol. Ital., 1, 77-92.

Cassinis G., Durand M. & Ronchi A. (2002) - The Permian and Triassic continental framework of Nurra (NW Sardinia). Rend. Soc. Paleontol. Ital., 1, 297-305.

Cassinis G., Durand M. & Ronchi A. (2003) - Permian-Triassic continental sequences of northwest Sardinia and south Provence: stratigraphic correlations and palaeogeographic implications. In: Decandia F.A., Cassinis G. & Spina A. (Eds.), Spec. Proc. Int. Meeting "Late Palaeozoic to Early Mesozoic events of Mediterranean Europe, and additional regional reports", Siena, 2001. Boll. Soc. Geol. It., Vol. Spec. 2, 119-129.

Cherchi A. & Trémolières P. (1984) - Nouvelles données sur l'évolution structurale au Mésozoïque et au Cénozoïque de la Sardaigne et leurs implications géodynamiques dans le cadre méditerranéen. C. R. Acad. Sci. II, 298(20), 889-894.

Cherchi A. & Schroeder R. (1985) - Mesozoic of NW Sardinia. Stratigraphy. In: Cherchi A. (Ed.), 19th Eur. Micropaleont. Coll., Sardinia, Oct. 1985 - Guidebook, pp. 44-56.

Citton P., Ronchi A., Maganuco S., Caratelli M., Nicosia U., Sacchi E. & Romano M. (2019) - First tetrapod footprints from the Permian of Sardinia and their palaeontological and stratigraphical significance. Geol. J., 54, 2084-2098. https://doi.org/10.1002/gj.3285.

Citton P., Ronchi A., Nicosia U., Sacchi E., Maganuco S., Cipriani A., Innamorati G., Zuccari C., Manucci F. & Romano M. (2020) - Tetrapod tracks from the Middle Triassic of NW Sardinia (Nurra region, Italy). Ital. J. Geosci., 139, 309-320. https://doi.org/10.3301/IJG.2020.07.

Cocco F., Oggiano G., Funedda A., Loi A. & Casini L. (2018) - Stratigraphic, magmatic and structural features of Ordovician tectonics in Sardinia (Italy): a review. J. Iber. Geol., 44(4), 619-639, https://doi.org/10.1007/s41513-018-0075-1.

Cortesogno L., Cassinis G., Dallagiovanna G., Gaggero L., Oggiano G., Ronchi A., Seno S. & Vanossi M. (1998) - The post-Variscan volcanism in Late Carboniferous-Permian sequences of Ligurian Alps, Southern Alps and Sardinia. Lithos, 45, 305-328.

Costamagna L.G. (2012) - Alluvial, aeolian and tidal deposits in the Lower to Middle Triassic "Buntsandstein" of NW Sardinia (Italy): A new interpretation of the Neo-Tethys transgression. Z. Dtsch. Ges. Geowiss., 163(2), 165-183.

Dart C.J., McClay K. & Hollings P.N. (1995) - 3D analysis of inverted extensional fault systems, southern Bristol Channel basin, UK. In: Buchanan, J.G., Buchanan, P.G. (Eds.), Basin Inversion. Geol. Soc. Spec. Publ., 88, 393-413.

DISS Working Group (2021) - Database of Individual Seismogenic Sources (DISS), Version 3.3.0: A compilation of potential sources for earthquakes larger than M 5.5 in Italy and surrounding areas. INGV, https://doi.org/10.13127/diss3.3.0.

Durand M. (1988) - Le Trias détritique du "Bassin du Sud-Est" – Paléogéographique et environments de dépôt. Géologie Alpine, Grenoble, Mém. H.s. 14, 69-78.

Durand M. (1993) - Un exemple de sédimentation continentale permienne dominée par l'activité de chenaux méandriformes: la Formation de Saint-Mandrier (Bassin de Toulon, Var). Géologie de la France, 2, 43-55.

Durand M. (2006) - The problem of the transition from the Permian to the Triassic Series in southeastern France: comparison with other Peritethyan regions. In: Lucas S. G., Cassinis G. & Schneider J.W. (Eds.), Non-Marine Permian Biostratigraphy an Biochronology. Geol. Soc., London, Spec. Publ., 265, 281-296.

Durand M. (2008) - Permian to Triassic continental successions in southern Provence (France): an overview. Boll. Soc. Geol. It., 127, 697-716.

Durand M. & Bourquin S. (2013) - Criteria for the identification of ventifacts in the geological record: A review and new insights. C. R. Geosci., 345, 111-125.

Durand M., Meyer R. & Avril G. (1989) - Le Trias détritique de Provence, du dome de Barrot et du Mercantour - (Exemples de sédimentation continentale en contexte anorogénique). Publications Association des Sédimentologistes Français, 6, 135 pp.

Fanucci F. & Morelli D. (2001) - Modalità e cause della deriva del Blocco Sardo-Corso. St. Trent. Sc. Nat.-Acta Geol., 77, 5-14.

Fontana D., Gelmini R. & Lombardi G. (1982) - Le successioni sedimentarie e vulcaniche carbonifere e permo-triassiche della Sardegna. Mem. Soc. Geol. It., 24, 183-192.

Fontana D., Neri C., Ronchi A. & Stefani C. (2001) - Stratigraphic architecture and composition of the Permian and Triassic siliciclastic succession of Nurra (Nortwestern Sardinia). In: Cassinis G. (Ed.), Permian continental deposits of Europe and other areas. Regional reports and correlations, Proceed. Intern. Field Conf. on "The continental Permian of the Southern Alps and Sardinia (Italy). Regional reports and general correlations", 15-25 Sept. 1999, Brescia, Italy: "Natura Bresciana", Annuali del Museo Civico di Scienze Naturali, Brescia, Monografia, 25, 149-161.

Funedda A., Oggiano G. & Pasci S. (2000) - The Logudoro Basin; a key area for the Tertiary tectono-sedimentary evolution of north Sardinia. Boll. Soc. Geol. It., 119(1), 31-38.

Gaggero L., Gretter N., Langone A. & Ronchi A. (2017) - U-Pb geochronology and geochemistry of late Palaeozoic volcanism in Sardinia (southern Variscides). Geosci. Front., 1-22, https://doi.org/10.1016/j.gsf.2016.11.015.

Gand G., Garric J., Demathieu G. & Ellenberger P. (2000) - La palichnofaune de vertébrés tétrapodes du Permien supérieur du bassin de Lodève (Languedoc, France). Paléovertebrata, 29, 1–82.

Gandin A., Pittau P. & Ronchi A. (2007) - Buntsandstein. In: Cita M.B., et al. (Eds.), Carta Geologica d'Italia 1:50.000. Catalogo delle formazioni - Unità tradizionali (2) Fascicolo VII. Quaderni del Servizio Geologico d'Italia, Serie III, 7(7), 361-367.

Gasperi G. & Gelmini R. (1980) - Ricerche sul Verrucano. 4. Il Verrucano della Nurra (Sardegna nord-occidentale). Mem. Soc. Geol. It., 20, 215-231.

Ghinassi M., Durand M., Ronchi A. & Stefani C. (2009) - Permian–Middle Triassic continental succession of NW Sardinia. In: Pascucci V. & Andreucci S. (Eds.), Field-Trip Guidebook, Pre-conference Trip FT3 27th IAS Meeting of Sedimentology, Alghero 20–23 September 2009, 37-50.

Glinzboeckel C. & Durand M. (1984) - Trias: Provence et chaines subalpines meridionales. In: Debrand-Passard S., Courbouleix S. & Lienhardt M.-J. (Eds.), Synthèse géologique du Sud-Est de la France. Vol. 1: Stratigraphie et paléogéographie. Mém. Bur. Rech. Géol. Min., 125, 99-100.

Gretter N., Ronchi A., López-Gómez J., Arche A., De la Horra R., Barrenechea J. & Lago M. (2015) - The Late Palaeozoic-Early Mesozoic from the Catalan Pyrenees (Spain): 60 Myr of environmental evolution in the frame of the western peri-Tethyan palaeogeography. Earth-Sci. Rev., 150, 679-708.

Hotton III N., Olson E.C. & Beerbower R. (1997) - Amniote origins and the discovery of herbivory. In: Sumida S.S. & Martin K.L.M. (Eds.), Amniote Origins, Completing the Transition to Land. Academic Press, San Diego, 207-264.

ITHACA Working Group (2019) - ITHACA (ITaly HAzard from CApable faulting), A database of active capable faults of the Italian territory. Accessible online at: http://sgi.isprambiente.it/ithaca/viewer (Accessed on July 1st 2023).

Kozur H.W. & Bachmann G.H. (2005) - Correlation of the Germanic Triassic with the international scale. Albertiana, 32, 21-35.

Lombardo M.P. (2008) - Access to mutualistic endosymbiotic microbes: an underappreciated benefit of group living. Behav. Ecol. Sociobiol., 62, 479-497.

Lovisato D. (1884) - Nota sopra il Permiano ed il Triassico della Nurra in Sardegna. Boll. Com. Geol. It, 15, 305-325.

Maidwell F.T. (1911) - Notes on footprints from the Keuper of Runcorn Hill. Proc. Liverpool Geol. Soc., 11, 140-152.

Menegoni N., Inama R., Crozi M. & Perotti C. (2022a) - Early deformation structures connected to the progradation of a carbonate platform: The case of the Nuvolau Cassian platform (Dolomites-Italy). Mar. Petrol. Geol., 138, 105574.

Menegoni N., Inama R., Panara Y., Crozi M. & Perotti C. (2022b) - Relation between fault and fracture network affecting the Lastoni di Formin carbonate platform (Italian Dolomites) and its deformation history. Geosciences, 12(12), 451. https://doi.org/10.3390/geosciences12120451.

Miall A.D. (2016) - The valuation of unconformities. Earth-Sci. Rev., 163, 22-71.

Michel L.A., Tabor N.J., Montañez I.P., Schmitz M.D. & Davydov V.I. (2015) - Chronostratigraphy and paleoclimatology of the Lodève Basin, France: evidence for a pan-tropical aridification event across the Carboniferous–Permian boundary. Palaeogeogr., Palaeocl., 430, 118-131.

Oggiano G., Aversano A., Forci A., Langiu M.R. & Patta E.D. (2018) - Note illustrative della carta geologica d'Italia alla scala 1:50.000, F. 459 Sassari, 193 pp. ISPRA, Roma.

Oggiano G., Funedda A., Carmignani L. & Pasci S. (2009) - The Sardinia-Corsica microplate and its role in the Northern Apennine Geodynamics: New Insights from the tertiary intraplate strike-slip tectonics of Sardinia. Ital. J. Geosci., 128(2), 527-539, https://doi.org/10.3301/IJG.2009.128.2.527.

Oggiano G., Pasci S. & Funedda A. (1995) - Il bacino di Chilivani-Berchidda; un esempio di struttura transtensiva, possibili relazioni con la geodinamica Caenozoica del mediterraneo occidentale. Boll. Soc. Geol. It., 114(2), 465-475.

Oosterbaan A.M. (1936) - Étude géologique et paléontologique de la Nurra avec quelques notes sur le Permien et le Trias de la Sardaigne meridionale: 130 pp., Utrecht University.

Panara Y., Menegoni N., Carboni F. & Inama R. (2022) - 3D digital outcrop model-based analysis of fracture network along the seismogenic Mt. Vettore Fault System (Central Italy): the importance of inherited fractures. J. Struct. Geol., 161, 104654, https://doi.org/10.1016/j.jsg.2022.104654.

Peabody F.E. (1948) - Reptile and amphibian trackways from the Moenkopi Formation of Arizona and Utah. Bull. Dep. Geol. Sci. Univ. California, 27, 295-468.

Pecorini G. (1962) - Nuove osservazioni sul Permico della Nurra (Sardegna nord-occidentale). Atti Accademia Nazionale dei Lincei, Rendiconti Classe di Scienze Fisiche, Matematiche e Naturali, 32, 377-380.

Pittau P. & Del Rio M. (2002) - Palynofloral biostratigraphy of the Permian and Triassic sequences of Sardinia. Rend. Soc. Paleontol. Ital., 1, 93-109.

Pittau Demelia P. & Del Rio M. (1980) - Pollini e spore del Trias medio e del Trias superiore negli affioramenti di Campumari e di Ghisciera Mala (Sardegna). Boll. Soc. Paleontol. Ital., 19, 241-249.

Pittau Demelia P. & Flaviani A. (1982) - Aspects of the palynostratigraphy of the Triassic Sardinia sequences (Preliminary report). Rev. Palaeobot. Palyno., 37, 329-43.

Pomesano Cherchi A. (1968) - Studio biostratigrafico del sondaggio Cugiareddu nel Trias e Permico della Nurra (Sardegna nord-occidentale). Pubblicazione dell'Istituto di Geologia e Paleontologia dell'Universitàdi Cagliari, 61, 51 pp.

Postpischl D. (1985) - Catalogo dei terremoti italiani dall'anno 1000 al 1980. Quaderni della Ricerca Scientifica, 114, 2B, Bologna, 239 pp.

Reisz R.R. & Sues H.D. (2000) - Herbivory in late Paleozoic and Triassic terrestrial vertebrates. In: Sues H.-D. (Ed.), Evolution of Herbivory in Terrestrial Vertebrates. Cambridge University Press, 9–41.

Romano M. (2017a) - Gut microbiota as a trigger of accelerated directional adaptive evolution: acquisition of herbivory in the context of extracellular vesicles, microRNAs and inter-kingdom crosstalk. Frontiers in Microbiology, 8, 721, https://doi.org/10.3389/fmicb.2017.00721.

Romano M. (2017b) - Long bone scaling of caseid synapsids: a combined morphometric and cladistic approach. Lethaia, 50, 511-526

Romano M. & Nicosia U. (2014) - *Alierasaurus ronchii*, gen. et sp. nov., a caseid from the Permian of Sardinia, Italy. J. Vertebr. Paleontol., 34(4), 900-913.

Romano M. & Nicosia U. (2015) - Cladistic analysis of Caseidae (Caseasauria, Synapsida): using the gap-weighting method to include taxa based on incomplete specimens. Palaeontology, 58, 1109- 1130.

Romano M. & Rubidge B. (2019) - Long bone scaling in Captorhinidae: do limb bones scale according to elastic similarity in sprawling basal amniotes? Lethaia, 52, 389-402

Romano M., Citton P., Maganuco S., Sacchi E., Caratelli M., Ronchi A. & Nicosia U. (2019) - New tetrapod discovery at the Permian outcrop of Torre del Porticciolo (Alghero, Italy). Geol. J., 54(3), 1554-1566, https://doi.org/10.1002/gj.3250.

Romano M., Ronchi A., Maganuco S. & Nicosia U. (2017) - New material of *Alierasaurus ronchii* (Synapsida, Caseidae) from the Permian of Sardinia (Italy), and its phylogenetic affinities. Palaeontol. Electron., 20.2.26A, 1-27.

Ronchi A., Broutin J., Diez J.B., Freytet P., Galtier J. & Lethiers F. (1998) - New paleontological discoveries in some Early Permian sequences of Sardinia. Biostratigraphic and paleogeographic implications. C. R. Acad. Sci., Paris, 327, 713-718.

Ronchi R., Sacchi E., Nicosia U. & Romano M. (2008) - Ritrovamento di un vertebrato di grandi dimensioni nei depositi continentali permiani della Nurra. Istituto Lombardo (Rendiconti di Scienze), 142, 291-306.

Ronchi A., Sacchi E., Romano M. & Nicosia U. (2011) - A huge caseid pelycosaur from north–western Sardinia and its bearing on European Permian stratigraphy and palaeobiogeography. Acta Palaeontol. Pol., 56(4), 723-738, https://doi.org/10.4202/app.2010.0087

Rovida A., Locati M., Camassi R., Lolli, B., Gasperini P. & Antonucci A. (2022) - Catalogo Parametrico dei Terremoti Italiani (CPTI15), versione 4.0. INGV, https://doi.org/10.13127/CPTI/CPTI15.4.

Schneider J.W., Lucas S.G., Scholze F., Voigt S., Marchetti L., Klein H., Opluštil S., Werneburg R., Golubev V.K., Barrick J., Nemyrovska T. & Ronchi A. (2020) - Report on the activities of the Late Carboniferous – Permian – Early Triassic Nonmarine-Marine Correlation Working Group for 2018 and 2019. Permophiles, 68, 35-40.

Sciunnach D. (2001) - Heavy mineral provinces as a tool for palaeogeographic reconstruction: A case study from the Buntsandstein of Nurra (NW Sardinia, Italy). Ecl. Geol. Helv., 94, 197-211.

Sues H.-D. & Reisz R.R. (1998) - Origins and early evolution of herbivory in tetrapods. Tr. Ecol. Evol., 13, 141-145.

Vardabasso S. (1966) - Il Verrucano sardo. Atti del Symposium sul Verrucano, Pisa sett. 1965, Società Toscana di Scienze Naturali, 293-310.

Zattin M., Massari F. & Dieni I. (2008) - Thermochronological evidence for Mesozoic–Tertiary tectonic evolution in the eastern Sardinia. Terra Nova, 20(6), 469-474, https://doi.org/10.1111/j.1365-3121.2008.00840.x.

Ziegler P.-A. & Stampfli G.-M. (2001) - Late Paleozoic-Early Mesozoic plate boundary reorganization: collapse of the Variscan orogen and opening of Neotethys. In: Cassinis G. (Ed.), Permian continental deposits of Europe and other areas. Regional reports and correlations. Museo Civico di Science Naturali di Brescia,17-34.